



A wide range kinetic modeling study of pyrolysis and oxidation of benzene



Chiara Saggese, Alessio Frassoldati, Alberto Cuoci, Tiziano Faravelli, Eliseo Ranzi *

Dipartimento di Chimica, Materiali ed Ingegneria Chimica "G. Natta" Politecnico di Milano, Piazza Leonardo da Vinci 32, 20133 Milano, Italy

ARTICLE INFO

Article history:

Received 27 November 2012
Received in revised form 30 January 2013
Accepted 13 February 2013
Available online 14 March 2013

Keywords:

Benzene kinetics
Detailed kinetics
Aromatics and soot

ABSTRACT

The aim of this work is to collect and review the vast amount of experimental data reported in recent years on benzene pyrolysis and oxidation and to analyze them by using and refining a detailed kinetic mechanism, thereby identifying a sensitive and crucial portion of the mechanism itself. Benzene is the first aromatic compound, a relevant intermediate of several combustion processes and also a key precursor to soot formation. The emphasis here is on high pressure pyrolysis experiments, ignition delay times in shock tubes, premixed flames as well as low temperature reactions with recombination and propagation reactions of cyclopentadienyl and phenoxy radicals playing a significant role. This is the first time the same kinetic model of benzene pyrolysis and oxidation has been compared with such a wide collection of experimental measurements.

© 2013 The Combustion Institute. Published by Elsevier Inc. All rights reserved.

1. Introduction

Benzene, aromatics and polycyclic aromatic hydrocarbons (PAH) are relevant intermediates of all practical combustion processes, and are also key precursors to soot formation [1–3]. Aromatic compounds are present in significant amounts in liquid fuels such as gasoline, diesel, kerosene, and jet fuels. They are used as anti-knock additives and improve resistance to auto-ignition, thus enhancing the octane number of the fuels. Real and commercial liquid fuels are complex and variable mixtures of several hydrocarbon species. Therefore, both in numerical simulations and in the experimental investigation of combustion processes, the complex real fuels are often simplified and represented by surrogates, in which aromatics are key components [4,5]. As a result, the proper kinetic understanding of the primary steps in the chemistry of aromatic species is also crucial to the kinetic modeling of surrogate mixtures.

Since the pioneering work of Brezinsky [6,7], the pyrolysis and oxidation reactions of benzene and alkyl aromatics have been widely debated and an extensive range of experimental data is now available in the literature.

The goal of this paper is to further validate a general detailed kinetic model [8,9] using the complete set of experimental data of benzene pyrolysis, oxidation and combustion. A similar effort was also recently made by Vourliotakis et al. [10] on benzene mechanism and by Metcalfe et al. [11] on toluene mechanism.

The refined kinetics of benzene oxidation will lay the basis not only for the extension of the scheme towards heavier aromatic fuels, but also for a better kinetic understanding of the successive growing processes of polycyclic aromatic hydrocarbons (PAH) and soot. The initial benzene conversion proceeds mainly through H-abstraction from benzene (C_6H_6) to form the phenyl radical (C_6H_5), followed by C_6H_5 oxidation to form the phenoxy radical (C_6H_5O). In addition to this, benzene may be oxidized directly with the oxygen atom to form phenol (C_6H_5OH), phenoxy, or CO and cyclopentadienyl radical (C_5H_5). At high temperatures, the phenoxy radical quickly decomposes to form CO and cyclopentadienyl, while at low temperatures recombination reactions of these radicals have a significant effect on the chemistry of benzene decomposition. Even from these simple features, it is clear that a hierarchical and modular approach to the chemistry of benzene and aromatics first demands a proper description of the pyrolysis and oxidation of cyclopentadiene and the C_5H_5 radical, as well as of phenol and the C_6H_5O radical. Reaction flux and sensitivity analyses of different reacting systems show the crucial role of specific reactions and interactions amongst phenyl, phenoxy and cyclopentadienyl radicals. While cyclopentadiene kinetics was discussed recently [12], the chemistry of phenol and phenoxy radical deserves a closer analysis and is discussed in brief in Appendix A, with some comparisons with experimental measurements relating to hydro-pyrolysis [13] and oxidation conditions [14,15].

Table 1 summarizes the experimental data relating to benzene. These include well-stirred [16–19] and flow reactors [14,20–22] at different operating pressures, shock tubes [19,23–28], rapid compression machines [29], batch reactors [30], burner stabilized flames, as well as counterflow and spherically expanding flames

* Corresponding author.

E-mail address: eliseo.ranzi@polimi.it (E. Ranzi).

Table 1

Summary of the experimental benzene pyrolysis, oxidation and combustion data analyzed in this work.

Operating conditions	Temperature (K)	Pressure (atm)	Equivalence ratio	Feed composition	Refs.
Jet Stirred Reactor (JSR)	950–1400	10	0.5–1.5	0.1–0.15 mol% in air	[16]
	900–1300	0.46	0.19, 1.02	0.51 mol% in Ar/O ₂	[17]
	950–1350	1	0.3–1.5	0.15 vol% in air	[18]
	923	1	1.9,3.6	4–4.5 mol% in He/O ₂	[19]
Plug Flow Reactor (PFR)	1120	1	0.39	0.078 mol% in air	[20]
	1100	1	0.76–1.36	0.16 mol% in air	[21]
	900–1450	1	0.002–1	Benzene/O ₂ /H ₂ O	[14]
	850–960	1	0.1–1.3	Benzene/O ₂ /N ₂	[22]
Shock Tube reactor (ST)	1704–2192	0.4–0.5	∞	Benzene/Ne	[23]
	1212–1748	1.7–7.89	0.25–2	0.42–1.69 mol% in O ₂ /Ar	[24]
	650–2200	4	1	0.5–11.7 mol% in Ar/O ₂	[25]
	1100–1300	13–39	1	2.7 mol% in air	[26]
	1400–2000	5	∞	0.3 mol% in Ar	[27]
	1230–1970	6.5–9.5	0.5–3	1.25–2.5 mol% in O ₂ /Ar	[19]
	1200–1800	30–50	∞	0.0065–0.08 mol% in Ar	[28]
Rapid Compression Machine (RCM)	920–1100	25–45	0.5–1	1 mol% in O ₂ /N ₂ /Ar	[29]
Batch reactor	773	0.66	0.005–0.05	0.05 mol% in O ₂ /N ₂ /H ₂	[30]
Flame speed	T _o = 298	1	0.7–1.7	Benzene/air flames	[31]
	T _o = 450	3	0.8–1.4	Benzene/air flames	[32]
	T _o = 353	1	0.7–1.5	Benzene/air flames	[3]
Premised flames	400–1600	0.03	1.8	Benzene/O ₂ /Ar flames	[33]
	500–1800	1	1.8	Benzene/air flames	[34]
	700–1800	0.05	2	Benzene/O ₂ /Ar flames	[35]
	450–1500	0.05	1	CH ₄ /1.5% benzene/O ₂ /N ₂	[36]
	600–1800	0.04	1.78	Benzene/O ₂ /Ar flames	[37]
	500–1750	0.045	0.7–2	Benzene/O ₂ /Ar flames	[38]
	1100–1810	1	1.98	Benzene/air flames	[39]

[3,31–39]. **Figure 1** shows an axonometric view of the wide range of analyzed experimental temperature, pressure and equivalence ratio conditions, with the related bi-dimensional sections. The different colors refer to different reactors and conditions (red¹: jet stirred reactor, yellow: plug flow reactor, green: shock tube, blue: rapid compression machine, cyan: flame conditions).

In a recent article [9], the kinetic scheme was shown to be capable of explaining the chemistry governing a large amount of experimental laminar flame speeds. Thus, the overall mechanism was used as a kinetic guideline useful in comparing and unifying flame speed data relating to similar fuels and/or conditions from different sources. This work also highlighted the importance of a further kinetic analysis of the sub mechanism of aromatic species. The previous kinetic scheme of the pyrolysis and oxidation of aromatic species [40] was mainly based on the very useful oxidation data provided by the Princeton flow reactor [6] and just a small amount of other data. The aim of this work is to collect and review the large amount of new experiments relating to benzene pyrolysis and oxidation (shown in **Table 1** and **Fig. 1**), analyze them by using and refining a detailed kinetic mechanism, and thereby identify sensitive and crucial portions of the mechanism itself. As a result, the kinetic model may also become a useful tool in comparing and unifying different sets of experimental measurements.

2. Kinetic model and numerical method

The detailed oxidation mechanism of hydrocarbons adopted here [9] consists of over 10,000 reactions and more than 350 species, and was developed based on hierarchical modularity. Thermochemical data for most species were obtained from the CHEMKIN thermodynamic database [41,42]. For those species whose thermodynamic data are not available in the literature,

the group additive method was used to estimate these properties [43].

All numerical simulations were performed using OpenSMOKE code, an upgraded version and extension of the well-tested DSMOKE code [44,45]. The BzzMath 6.0 numerical library was adopted [46,47]. A mixture-averaged formula was also used to compute multicomponent diffusion coefficients. The conservation equations with proper boundary conditions [48] were discretized by means of conventional finite differencing techniques with non-uniform mesh spacing for the simulation of premixed laminar flames. Further details on the numerical methods are reported in [9,49].

The normalized sensitivity coefficient s_Y is used instead of the raw coefficient S_Y :

$$s_Y = \frac{\partial \ln Y}{\partial \ln \alpha} = \frac{\alpha \partial Y}{Y \partial \alpha} = \frac{\alpha}{Y} S_Y$$

where Y is the species concentration and α the generic frequency factor.

Table 2 reports the major reactions discussed in this work, while the overall kinetic model, with thermo and transport properties, is available in CHEMKIN format from: <http://creckmodeling.chem.polimi.it>.

3. Model validation and comparison with experimental measurements

As already discussed and presented in **Table 1** and **Fig. 1**, all of the experimental data are organized into the following five different sets of data and operating conditions for the sake of convenience:

1. Shock tube experiments of benzene pyrolysis.
2. Benzene pyrolysis and oxidation in flow reactors.
3. Ignition delay time of benzene oxidation.

¹ For interpretation of color in Fig. 1, the reader is referred to the web version of this article.

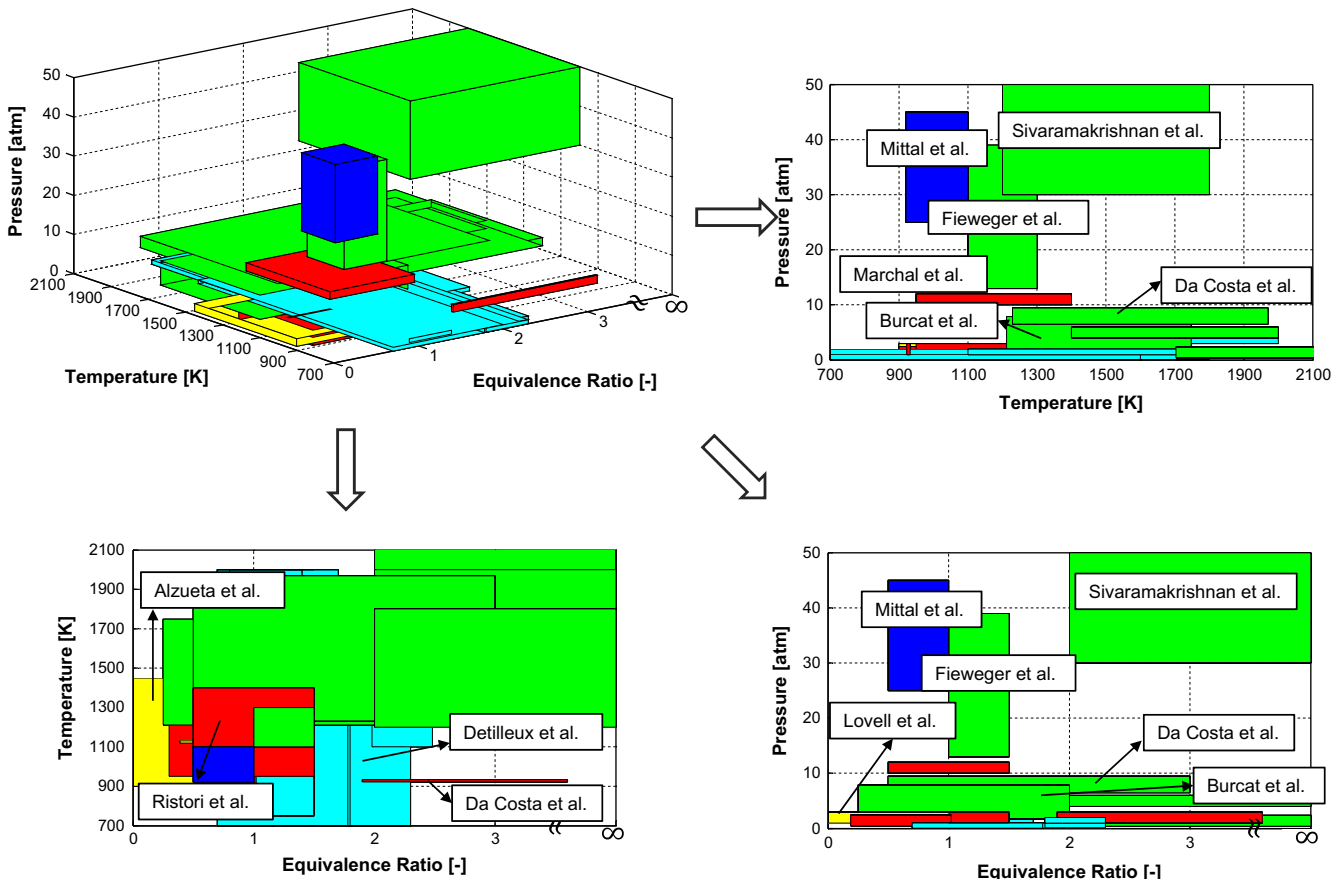


Fig. 1. Axonometric and bi-dimensional views of the wide range of the analyzed experimental conditions from Table 1.

4. Partial oxidation and combustion in jet stirred reactors.
5. Premixed laminar flames.

3.1. Shock tube experiments of benzene pyrolysis

Three different sets of benzene pyrolysis in shock tube experiments are analyzed here. The first refers to the pyrolysis of a benzene–Ne mixture at 1704–2192 K and pressure 0.367–0.516 atm [23]. The second set of experiments was performed in the temperature range 1400–2000 K by Laskin and Lifshitz [27], and the third refers to the high pressure (30–50 bar) experiments of Sivaramakrishnan et al. [28].

The C–H bonds in benzene are weaker than the C–C bond in the ring [61]. Thus, the initiation step in benzene pyrolysis is the release of a hydrogen atom by breaking one of the C–H bonds in the molecule.



The H abstraction reaction of H atom to form phenyl radical significantly contributes to benzene decomposition:



At temperatures higher than 1400 K, the phenyl radical decomposition rate increases, and C_2H_2 and C_4H_2 become the main decomposition products. Thermal decomposition of benzene was originally described by the Bauer-Aten mechanism [62] based on the successive formation and decomposition of C_6H_5 and C_4H_3 radicals. In agreement with Colket [63] and Lindstedt and Skevis [52], the initial formation of a linear C_6H_5 radical is assumed as a third body reaction:



The kinetic parameters of this reaction were selected on the basis of the values proposed by Laskin and Lifshitz [27] and Sivaramakrishnan et al. [28]. Based on the findings of Wang et al. [58], the dehydrogenation reaction of phenyl to form *ortho*-benzyne (*o*- C_6H_4) and its successive decomposition is a favored phenyl decomposition path:



C_2H_2 and C_4H_2 are then the main stable decomposition products.

The addition on benzene and the recombination reaction of C_6H_5 lead to the formation of biphenyl ($\text{C}_{12}\text{H}_{10}$):



The self-reaction between phenyl radicals has been recently investigated by [64–66]. Their theoretical results indicate the presence of a minor reaction channel leading to the formation of benzene and *o*-benzyne:

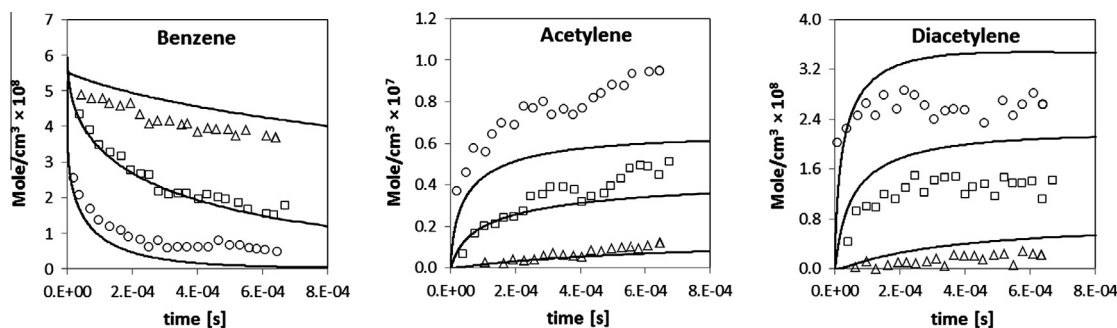


Figure 2 shows a first comparison of predicted and measured mole fractions of benzene, acetylene and diacetylene in the shock tube experiments of 2.1% benzene–Ne mixture at 1704, 1942 and 2192 K [23]. The model largely under predicts acetylene at high temperatures but also indicates significant formation of C_6 and

Table 2

Major reactions of benzene and phenol discussed in this work.

Reactions	$k = A \exp(-E_a/RT)^a$	A	E_a	Refs.
<i>Benzene reactions</i>				
R1	$H + C_6H_5 \leftrightarrow C_6H_6$	8.5×10^{10}	0	[50]
R2	$H + C_6H_6 \leftrightarrow H_2 + C_6H_5$	1.5×10^{11}	10,000	This work
R3	$OH + C_6H_6 \leftrightarrow H_2O + C_6H_5$	2.0×10^{10}	5000	This work
R4	$O + C_6H_6 \leftrightarrow OH + C_6H_5$	1.6×10^{11}	12,750	[51]
R5	$HO_2 + C_6H_6 \leftrightarrow H_2O_2 + C_6H_5$	6.4×10^9	25,600	[51]
R6	$CH_3 + C_6H_6 \leftrightarrow CH_4 + C_6H_5$	4.6×10^9	14,600	[51]
R7	$aC_3H_5 + C_6H_6 \leftrightarrow C_3H_6 + C_6H_5$	2.85×10^9	28,300	[51]
R8	$O_2 + C_6H_6 \leftrightarrow HO_2 + C_6H_5$	6.3×10^{10}	60,000	[52]
R9	$O + C_6H_6 \leftrightarrow C_6H_5O + H$	1.5×10^{10}	4000	[14]
R10	$OH + C_6H_6 \leftrightarrow C_6H_5OH + H$	4.5×10^9	8400	[50,13]
R11	$C_3H_3 + C_3H_3 + M \leftrightarrow C_6H_6 + M$	$k_{\infty} = 3.0 \times 10^9$	0	[53] ^b
R12	$C_2H + C_6H_6 \leftrightarrow H + C_8H_6$	1.0×10^9	0	[54]
<i>Phenyl radical reactions</i>				
R13	$C_6H_5 + M \leftrightarrow l-C_6H_5 + M$	3.0×10^{14}	67,000	This work
R14	$l-C_6H_5 \rightarrow C_2H_2 + C_4H_3$	1.0×10^{14}	38,000	[28] ^c
R15	$l-C_6H_5 \rightarrow 2 C_2H_2 + C_2H$	2.0×10^{14}	38,000	[28] ^c
R16	$O_2 + C_6H_5 \leftrightarrow C_6H_5O + O$	2.6×10^{10}	6120	[55]
R17	$O_2 + C_6H_5 \rightarrow OC_6H_4O + OH$	1.0×10^{10}	9000	[55] ^b
R18	$HO_2 + C_6H_5 \leftrightarrow C_6H_5O + OH$	2.0×10^{10}	1000	[52] ^b
R19	$C_3H_3 + C_3H_3 \leftrightarrow C_6H_5 + H$	3.0×10^9	0	[53] ^b
R20	$C_6H_5 + C_2H_2 \leftrightarrow H + C_8H_6$	2.0×10^9	8000	[53] ^b
R21	$C_6H_5 + C_6H_6 \leftrightarrow H + C_{12}H_{10}$	1.0×10^8	4000	[56] ^b
R22	$C_6H_5 + C_6H_5 \leftrightarrow C_{12}H_{10}$	5.0×10^9	0	[57]
R23	$C_6H_5 + C_6H_5 \leftrightarrow C_6H_6 + o-C_6H_4$	5.0×10^8	0	This work
R24	$C_6H_5 \rightarrow o-C_6H_4 + H$	4.5×10^{13}	72,500	[58]
R25	$o-C_6H_4 \leftrightarrow C_2H_2 + C_4H_2$	1.0×10^{17}	88,000	[58] ^b
R26	$H + C_8H_6 \leftrightarrow H_2 + C_8H_5$	1.8×10^{11}	14,500	[51]
R27	$C_8H_5 + C_2H_2 \rightarrow C_{10}H_7$	1.0×10^9	5000	[54]
<i>Phenol and phenoxy radical reactions</i>				
R28	$C_6H_5O \leftrightarrow C_5H_5 + CO$	2.0×10^{11}	43,920	[50]
R29	$H + C_6H_5O + M \leftrightarrow C_6H_5OH + M$	$k_{\infty} = 4.0 \times 10^{11}$	0	[50]
R30	$H + C_6H_5O \leftrightarrow C_5H_6 + CO$	2.0×10^{11}	0	This work
R31	$O + C_6H_5O \leftrightarrow OC_6H_4O + H$	1.0×10^{11}	0	[14]
R32	$C_6H_5OH \leftrightarrow C_5H_6 + CO$	2.5×10^{13}	72,400	[59]
R33	$H + C_6H_5OH \leftrightarrow H_2 + C_6H_5O$	8.9×10^{10}	10,700	[51]
R34	$OH + C_6H_5OH \leftrightarrow H_2O + C_6H_5O$	1.5×10^{10}	4800	[19]
R35	$O + C_6H_5OH \leftrightarrow OH + C_6H_5O$	5.0×10^{10}	9000	[51]
R36	$HO_2 + C_6H_5OH \leftrightarrow H_2O_2 + C_6H_5O$	2.0×10^9	18,000	[51]
R37	$CH_3 + C_6H_5OH \leftrightarrow CH_4 + C_6H_5O$	1.45×10^9	12,000	[51]
R38	$aC_3H_5 + C_6H_5OH \leftrightarrow C_3H_6 + C_6H_5O$	9.0×10^8	22,200	[51]
R39	$O_2 + C_6H_5OH \leftrightarrow HO_2 + C_6H_5O$	6.3×10^{10}	49,000	[51]
R40	$C_6H_5O + C_6H_5O \rightarrow C_{12}H_8O + H_2O$	4.0×10^{10}	11,000	[60] ^c

^a Units are: mole, l, s, K and cal.^b Adjusted to maintain the similarities and analogies amongst similar reactions.^c See text.**Fig. 2.** Comparison of predicted (lines) and measured (symbols) mole fractions of benzene, C_2H_2 and C_4H_2 from shock tube experiments of 2.1% benzene–Ne mixtures at 1704 (triangles), 1942 (squares) and 2192 K (circles) [23].

heavier species. In fact, aside from biphenyl and phenyl–acetylene, large amounts of naphthalene, pyrene and heavier species are formed as a result of the successive addition and cyclization reactions of the acetylenic species.

These components are also reported by Laskin and Lifshitz [27] in their study of the thermal decomposition of benzene behind reflected shocks in a pressurized driver single-pulse shock tube in the temperature range 1400–2000 K and contact times of ~ 2 ms.

Aside from C_2H_2 and C_4H_2 , phenyl-acetylene (C_8H_6 , i.e. $C_6H_5-C\equiv CH$), biphenyl ($C_{12}H_{10}$), and small quantities of C_6H_4 and C_6H_2 (more stable than C_6H_4), were also detected. Figure 3 shows a comparison between experimental data and model predictions. Due to the high activation energy involved in the opening of the phenyl ring (~72 kcal/mol), the main product at low temperatures is biphenyl, while at higher temperatures, the opening of the phenyl radical becomes the main reaction path. C_2H_2 and C_4H_2 become the main decomposition products, together with C_6H_2 .

Figure 4 shows the reaction path analysis at 1700 K and 25% benzene conversion. Phenyl radical is mostly formed through the H abstraction reaction (R2), and only 10–15% via the initiation reaction (R1). The successive reaction paths of phenyl radical to form *o*-benzyne (R24) and *l*- C_6H_5 (R13), are of similar importance. Phenyl depletion due to the formation of phenyl-acetylene (R20) and biphenyl ((R21) and (R22)) accounts for ~15%, in these conditions. The phenyl acetylene formation is due mainly to phenyl addition to acetylene:



Only a minor role is played by the direct addition of C_2H radical to benzene:



Further recombination and addition reactions of phenyl radical with C_3 and C_4 species contribute to the formation of indene, indenyl and naphthalene. According to the HACA mechanism [53], successive H abstractions and addition reactions of acetylene explain the formation of C_{10} and heavier aromatic species:



The kinetic model predicts more than 30% (on a carbon basis) naphthalene, phenanthrene, pyrene and heavier aromatic species, at 1700 K and 1 ms.

The third set of experiments refers to high-temperature benzene pyrolysis in the high pressure shock tube at UIC [28]. Three sets of experiments were performed at nominal pressures of 30 and 50 bars, temperatures ranging from 1200 to 1800 K, and reaction times in the order 1.2–1.5 ms. Reagent mixtures consisting of benzene, 65–800 ppm diluted in Argon, were more dilute than the previous study [27] by one order of magnitude thereby minimizing second order reactions. Nevertheless, significant amounts of soot and PAH are known to be produced under these high pressure and temperature conditions [67]. Thus, significant loss of material, up to 50% deviations from the total carbon, was experimentally observed at higher temperatures. Even in the simplest case of benzene chemistry these simulations reflect the complexity and

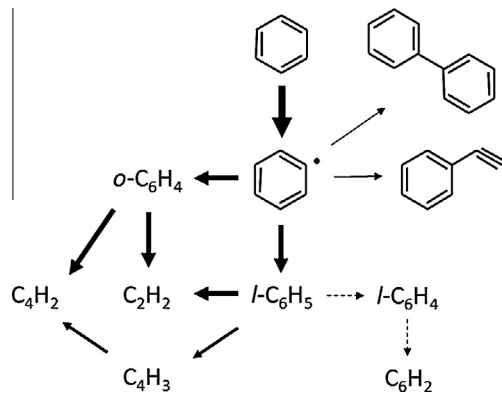


Fig. 4. High temperature pyrolysis of benzene. Reaction path analysis at 1700 K and 25% conversion [27]. The thickness of the arrows reflects the relative significance of the different reaction paths.

uncertainty of describing primary decomposition steps and the successive high-temperature reactions. Despite a systematic underprediction of benzene decomposition, Figure 5 demonstrates that the model agrees reasonably well with these high pressure data. Phenyl radical is again formed with the H abstraction reaction (R2) together with the initiation reaction (R1). As already discussed by Sivaramakrishnan et al. [28], sensitivity analysis shows a larger sensitivity coefficient to the phenyl decyclization reaction to form the linear C_6H_5 radical (R13) and this is the prevailing reaction path, at high pressures. In contrast there is a less sensitivity to the dehydrogenation reaction of phenyl radical to form *o*- C_6H_4 (R24), which is more favored at lower pressures. The model reasonably predicts benzene decay and C_2H_2 formation, but significantly overpredicts the formation of C_4H_2 , as also observed by Sivaramakrishnan et al. [28]. The model predicts significant formation of phenyl-acetylene, again via (R20). As expected, lower amounts of naphthalene and heavier species are formed under these conditions. The recent work of Comandini and Brezinsky [68] on the possible role of phenyl–phenyl addition to form naphthalene and acetylene, via isomerization of biphenyl radicals and the formation of benzobicyclo[2.2.2]octatriene also highlights the ongoing interest in heavy species formation.

Figure 6 shows a comparative sensitivity analysis of reaction rates on benzene concentration for the three sets of investigated experimental data [23,27,28], at about 1700 K and 25% benzene conversion.

(R1) and (R2) are always the most sensitive reactions. The relative importance of phenyl decomposition to form *o*- C_6H_4 or *l*- C_6H_5 is strictly related to pressure conditions. Therefore, *o*- C_6H_4

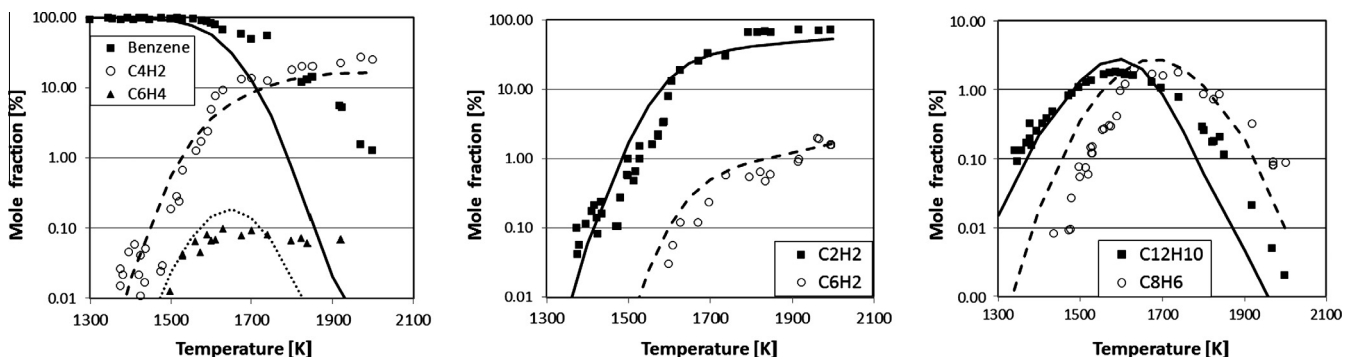


Fig. 3. High temperature pyrolysis of benzene [27]. Experimental (symbols) and predicted mole percent (lines) as a function of temperature (K).

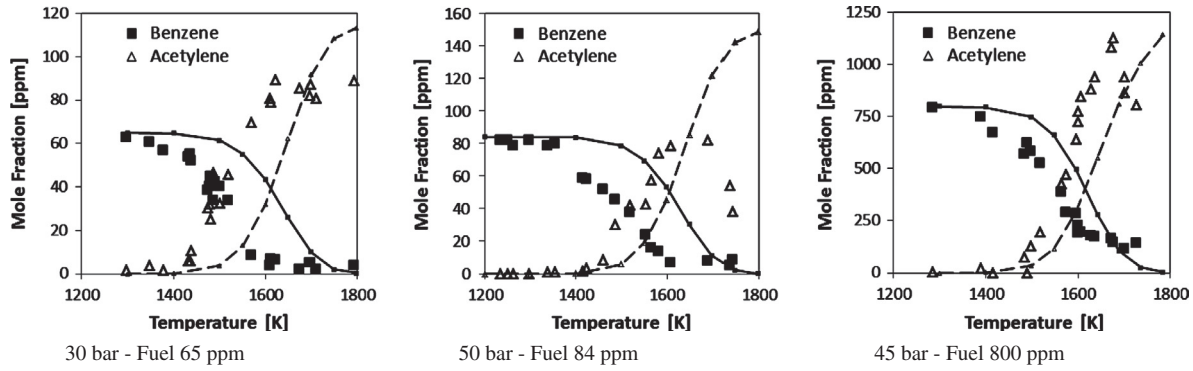


Fig. 5. High pressure pyrolysis of benzene [28]. Experimental (symbols) and predicted mole fractions (lines) as a function of temperature (K) for three different operating conditions.

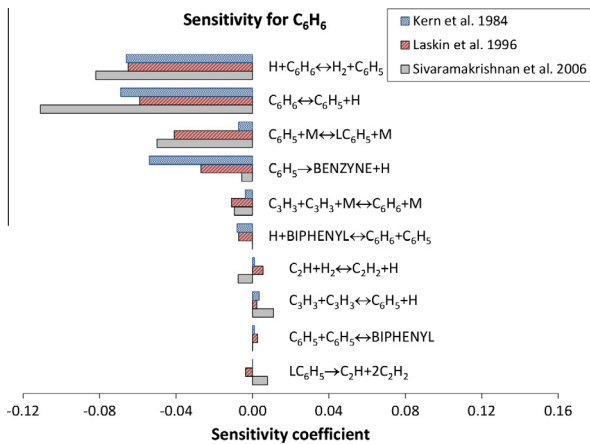


Fig. 6. Sensitivity coefficients of benzene concentration on reaction rate coefficients, at about 1700 K and 25% benzene pyrolysis.

formation has the highest sensitivity coefficient in the experiments of Kern et al. [23], while the *l*-C₆H₅ formation prevails in the high pressure experiments [28]. The high temperature conditions of this sensitivity analysis reduce the importance of the biphenyl formation reactions. Benzene decomposition reactions to form propargyl radicals:



as well as the self recombination of the resonantly stabilized propargyl radicals with C₆H₅ formation (R19) highlight the role of the C₃ species in the first aromatic ring formation and decomposition.

Summarizing the comparisons of the pyrolysis data, the model is a compromise between the different sets of experimental information.

3.2. Benzene pyrolysis and oxidation in flow reactors

Two different sets of data relating to plug flow reactors are analyzed in this paragraph. They refer to the flow reactor at Princeton [6], and the flow reactor at Lyngby [14], both operating at nearly atmospheric pressure and with a contact time of ~0.12–0.15 s.

3.2.1. Pyrolysis and oxidation in the Princeton flow reactor

Aromatic hydrocarbon pyrolysis and oxidation were extensively studied in the Princeton flow reactor at temperatures up to 1200 K and all this activity was critically reviewed by Brezinsky [6]. Parallel to the H abstraction reactions to form phenyl radical

[21], benzene oxidation mainly proceeds via O and OH radical addition to the ring to produce phenol and the phenoxy radical.



Furthermore, with low O and H radical concentrations the reaction of the phenyl radical with molecular oxygen is a significant source of phenoxy radicals. Subsequent C₆H₅O pyrolysis leads to CO and cyclopentadienyl radical. Successive O attack on C₅H₅ leads to ring opening and C₄H₅ formation.

The phenyl radical addition to O₂ leads to benzoquinone (OC₆H₄O) formation:



and we assume a kinetic constant of 10¹⁰exp(−9000/RT) (l/mol/s), lower than the value suggested by Frank et al. [55]. As already established by Alzueta et al. [14], the reaction of phenoxy radical with an O atom forms benzoquinone:



Both these reactions are fuel-specific sensitive reactions in the laminar flame speed of benzene and aromatic species. The formation of the two benzoquinone isomers is supported by the ab initio study of Lin and Mebel [70] and by Buth et al. [71]. The two benzoquinone isomers are lumped into a single equivalent species.

Figure 7 shows the profiles of benzene and major products of the atmospheric oxidation of benzene at $\Phi = 0.76$ and $\Phi = 1.36$ and ~ 1100 K in the Princeton plug flow reactor [21]. In line with the suggestions of Zhao et al. [72], the experiments are conveniently modeled as an isobaric and adiabatic plug flow reactor only after the initial mixing zone and the experimental data were shifted by 30 ms. Figure 8 shows the main reaction paths in benzene oxidation at $\Phi = 1.36$ and benzene conversion of 15%. The thickness of the arrows reflects the relative importance of the different reaction paths. The important role played by the cyclopentadienyl radical, both with the oxidation and decomposition reactions to form CO and C₂ and C₄ species, and with the recombination reaction to form naphthalene is quite clear. The model properly reflects the relative amount of main products even though a systematic under prediction of overall benzene reactivity is observed. The predicted conversion agrees better with the similar benzene oxidation data of Venkat et al. [20], which are not here reported.

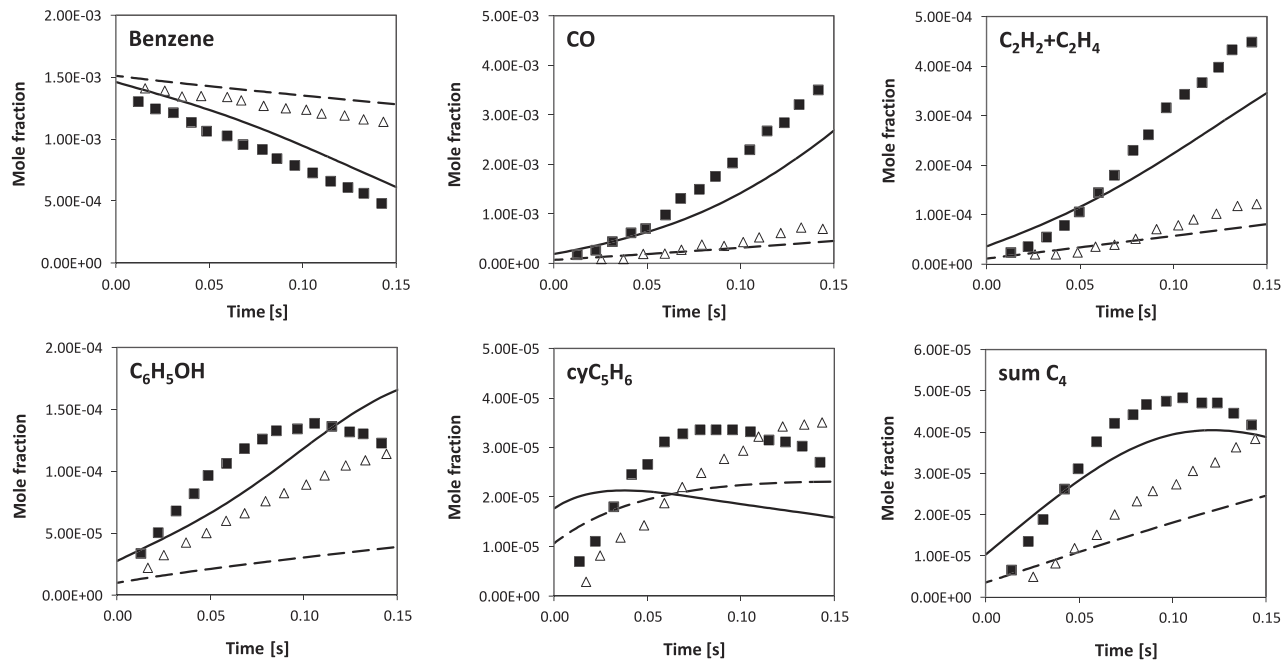


Fig. 7. Profiles of benzene and main products from the oxidation of benzene at ~ 1100 K in the Princeton plug flow reactor [21]. Experimental data ($\Phi = 0.76$: squares, $\Phi = 1.36$: triangles), model predictions (solid and dashed lines).

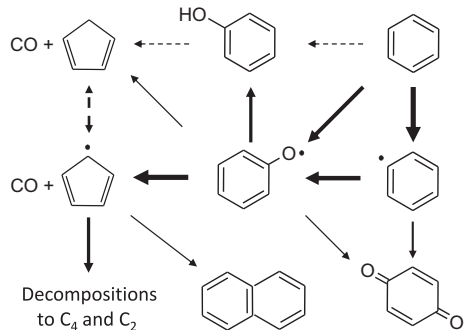


Fig. 8. Main reaction paths in benzene oxidation in the Princeton flow reactor. The thickness of the arrows reflects the relative significance of the different reaction paths at $\Phi = 1.36$ and 15% benzene conversion.

3.2.2. Near stoichiometric and very lean oxidation of benzene in the Lyngby flow reactor

Benzene oxidation under flow-reactor conditions with excess air ratios ranging from stoichiometric to very lean conditions was performed by Alzueta et al. [14]. The temperature range was 900–1450 K and the residence time was again of the order of 150 ms. Figure 9 shows a comparison between experimental data and model predictions for the mole fractions of benzene, CO, and CO_2 during the oxidation of benzene at $\lambda = 1.04$ and $\lambda = 49.6$ as a function of temperature. The model slightly over-estimates benzene reactivity in lean conditions at 1000–1100 K, while it agrees quite well with the experimental measurements in the near-stoichiometric conditions.

This over prediction is in contrast with the under prediction of benzene conversion in the Princeton reactor seen in Fig. 7 [21].

3.3. Shock tube experiments and ignition delay times of benzene oxidation

Three independent sources of experimental ignition delay times of benzene mixtures are analyzed here with pressure ranging from

2.44 up to 39 atm. The conditions investigated are summarized in Table 3.

The ignition delay times of benzene with oxygen diluted in argon were investigated by Burcat et al. [24] over a wide range of experimental conditions with benzene concentrations of 0.4–1.69%, fuel equivalence ratios of 0.25–2, in the temperature range 1212–1748 K and shock pressures from 1.7 to 7.89 atm.

As can be seen from panels a and b of Fig. 10, the model predicts the individual ignition delays as a result of the effect of both the equivalence ratio and pressure reasonably well. The apparent effect of pressure shown in panel b is indeed due to the increased fuel concentration in the experiments at higher pressure (see Table 3). Sensitivity analysis confirms that the ignition delay times are mostly sensitive to the kinetics of a limited number of specific reactions, still mostly involving phenyl, phenoxy and cyclopentadienyl radicals.

Similarly, the ignition delay times of benzene–oxygen–argon mixtures with fuel equivalence ratios from 0.5 to 3 were measured behind shock waves by Da Costa et al. [19] at temperatures from 1230 to 1970 K and pressures from 6.5 to 9.5 atm. Panel c of Fig. 10 compares the measured and predicted autoignition delay times as a function of temperature for different equivalence ratios at 1.25% benzene concentration and pressures from 6.5 to 9.5 atm. Panel d analyzes the effect of fuel concentration at $\Phi = 1$. There is a broad scatter in the experimental measurements and the model now seems to underestimate the apparent activation energy, a deviation not observed in the comparisons with the Burcat data.

The last set of data (see panel e) refers to the high pressure shock experiments of [26] in the temperature range 1000–1300 K. Contrary to the previous comparisons, the apparent activation energy now seems over-predicted with respect to the experimental one.

3.4. Partial oxidation and combustion in jet stirred reactors

As already shown in the Table 1 and Fig. 1, there are several experimental data also relating to the benzene oxidation in jet

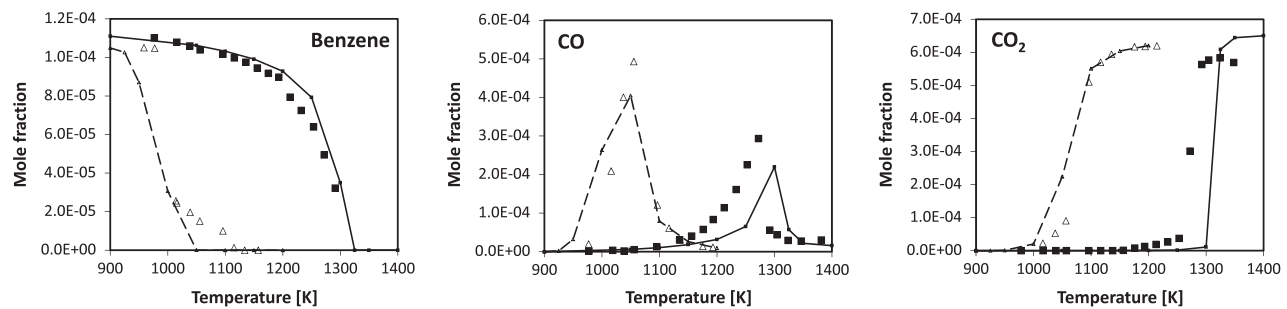


Fig. 9. Comparison between experimental data (symbols) and model predictions (lines with small symbols) for benzene, CO, and CO₂ during benzene oxidation at $\lambda = 1.04$ (squares) and $\lambda = 49.6$ (triangles) as a function of temperature [14].

Table 3
Operating conditions for the shock tube experiments analyzed in Fig. 10.

Mole fractions	Mixture	Equivalence ratio (ϕP)	Pressure after shock (atm)	Reflected temperature (K)	Refs.
C ₆ H ₆	O ₂				
0.0169	0.12675	Ar	1	2.1–3.0	[24]
0.0135	0.0509	Ar	2	2.1–3.0	1366–1748
0.0135	0.2031	Ar	0.5	1.9–2.7	1212–1488
0.00419	0.1257	Ar	0.25	1.7–2.4	1265–1560
0.0516	0.0387	Ar	1	5.7–7.9	1349–1652
0.0125	0.09375	Ar	1	7.8–9.3	1303–1579
0.0125	0.1875	Ar	0.5	8.1–9.4	1290–1418
0.0125	0.0625	Ar	1.5	6.3–8.5	1391–1659
0.0125	0.03125	Ar	3	7.4–7.8	1797–1970
0.0250	0.1875	Ar	1	8.5–9.51	1231–1362
0.02725	0.20436	N ₂	1	13	1100–1300
0.02725	0.20436	N ₂	1	39	1100–1300

stirred reactors, in a temperature range 900–1400 K and 0.46 up to 10 atm.

3.4.1. Atmospheric partial oxidation and combustion in jet stirred reactors

Several experimental results for benzene oxidation in an atmospheric pressure jet-stirred reactor at high temperatures (950–1350 K) and variable equivalence ratio (0.3, 0.5, 1 and 1.5) were reported by Ristori et al. [18]. These steady state experiments were performed at a constant mean residence time of 0.07 s, with a high degree of N₂ dilution (1000–1500 ppm vol. of fuel), which thereby reduces heat release and temperature gradients in the JSR.

Figure 11 compares experimental data and model predictions in lowest and maximum equivalent ratio conditions. Contrary to the previous data from the plug flow reactor, the model slightly overestimates the system reactivity, mostly in lean conditions. Predicted trends for main species reasonably agree with the experimental data. Figure 12 reports and compares the sensitivity analysis of benzene at equivalence ratios 0.3 and 1.5. The crucial role of phenol and cyclopentadiene, together with phenoxy and cyclopentadienyl radicals, is highlighted once again [10].

The sensitivity analysis performed in lean conditions shows that the over predicted benzene reactivity is mostly due to the decomposition of phenoxy radical to form CO and C₅H₅ radical:



the H abstraction reaction on benzene from OH:



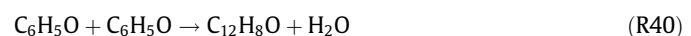
and the phenoxy radical oxidation to form benzoquinone (R31). While in rich conditions the major reaction paths responsible for

the higher benzene reactivity are the H abstraction reactions on benzene, and the oxidation and recombination reactions of C₅H₅ radical.

3.4.2. High pressure partial oxidation and combustion in jet stirred reactors

The kinetic model was also tested against the high pressure data of Marchal et al. [16] obtained in the previous stirred reactor [18]. These data refer to 10 atm, residence time of 0.7 s, over a wide range of temperatures (900–1200 K) and equivalence ratios (0.5–1.5). As can be seen from Fig. 13, the model overpredicts benzene conversion, but is still able to reproduce the pressure and stoichiometry effects and the main trends of the experimental data. Figure 14 shows the main reaction paths in benzene oxidation at 1000 K, $\phi = 1.5$, and benzene conversion of 50%. The thickness of the arrows reflects the relative importance of the different reaction paths and, at this high pressure and intermediate temperature, the important role played by the recombination reactions of phenoxy radicals forming heavier species is quite clear.

The recombination of phenoxy radicals with H₂O elimination can form dibenzofuran [60]:



The kinetic parameters suggested by Grotheer and Louw [60] were reduced and a parallel lumped recombination reaction with the intermediate formation of dialin (C₁₀H₁₀) was also considered. Both benzofuran and dialin are thus responsible for naphthalene formation. The high temperature CH₄ formation in rich conditions (Fig. 13) is mainly due to ethylene and vinyl radical oxidation to form ketene which adds H atoms and decomposes with methyl formation.

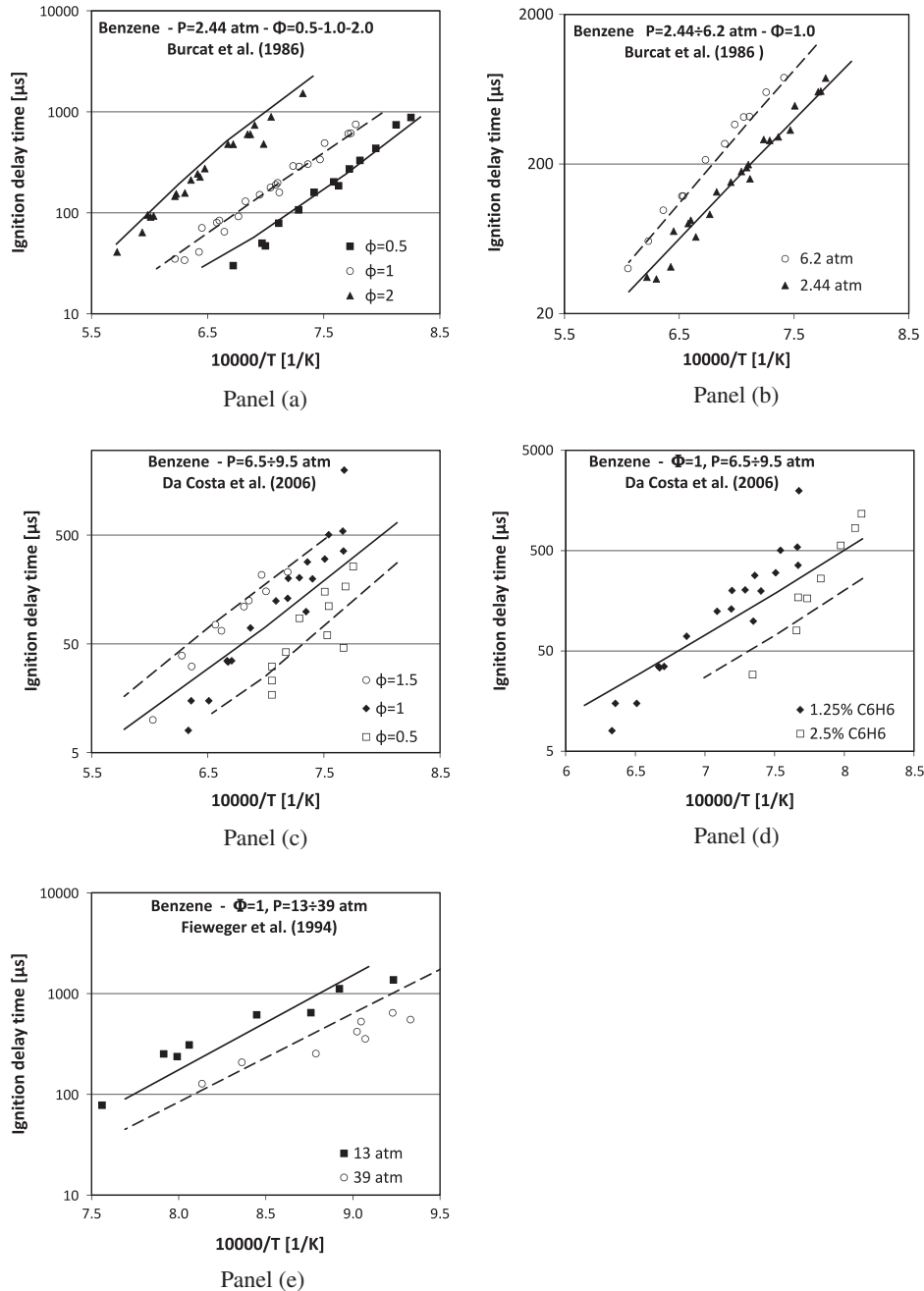


Fig. 10. Autoignition delay times of benzene oxidation as a function of temperature (K) behind reflected shock waves. Comparisons between experimental data (symbols) and predicted values (lines). (Panel a) Benzene–O₂–Ar mixtures: effect of equivalence ratio with fuel concentrations of 1.35–1.69% [24]. (Panel b) Benzene–O₂–Ar mixtures: effect of pressure at $\Phi = 1$ [24]. (Panel c) Benzene–O₂–Ar mixtures at 1.25% benzene, pressures from 6.5 to 9.5 atm and different equivalence ratios [19]. (Panel d) Benzene–O₂–Ar mixtures at $\Phi = 1$ and pressures from 6.5 to 9.5 atm with 1.25% and 2.5% benzene [19]. (Panel e) Benzene–O₂–N₂ mixtures at $\Phi = 1$ with pressure 13 and 39 atm [26].

3.4.3. Low temperature, partial oxidation of benzene in a jet stirred reactor

Low-temperature partial oxidation of benzene was studied by Da Costa et al. [19] in a continuous jet-stirred quartz reactor with an internal volume of 88 cm³. The mole compositions of the reacting flow were helium/oxygen/benzene = 80.5:15.5:4 (equivalence ratio $\Phi = 1.9$) and 86.1:9.4:4.5 ($\Phi = 3.6$). Experiments were carried out at a constant temperature (923 K) and atmospheric pressure, with residence times ranging from 1 to 10 s. The main products analyzed by gas chromatography were phenol, carbon monoxide and dioxide, methane, C₂ species (acetylene and ethylene were

not separated), propyne, propene, and 1,3-butadiene. These conditions are particularly mild (corresponding to benzene conversions of under 50%) compared with the ones of the previous stirred reactor and provide useful information on the relative role of the decomposition and recombination reactions of the phenoxy radical. Figure 15 shows the comparisons between experimental and predicted mole fractions of the main species. Phenol yields are properly predicted but the model systematically overestimates benzene conversion and C₂ species, which come mainly from successive decomposition reactions of benzoquinone and the cyclopentadienyl radical. Similar reactivity deviations were also

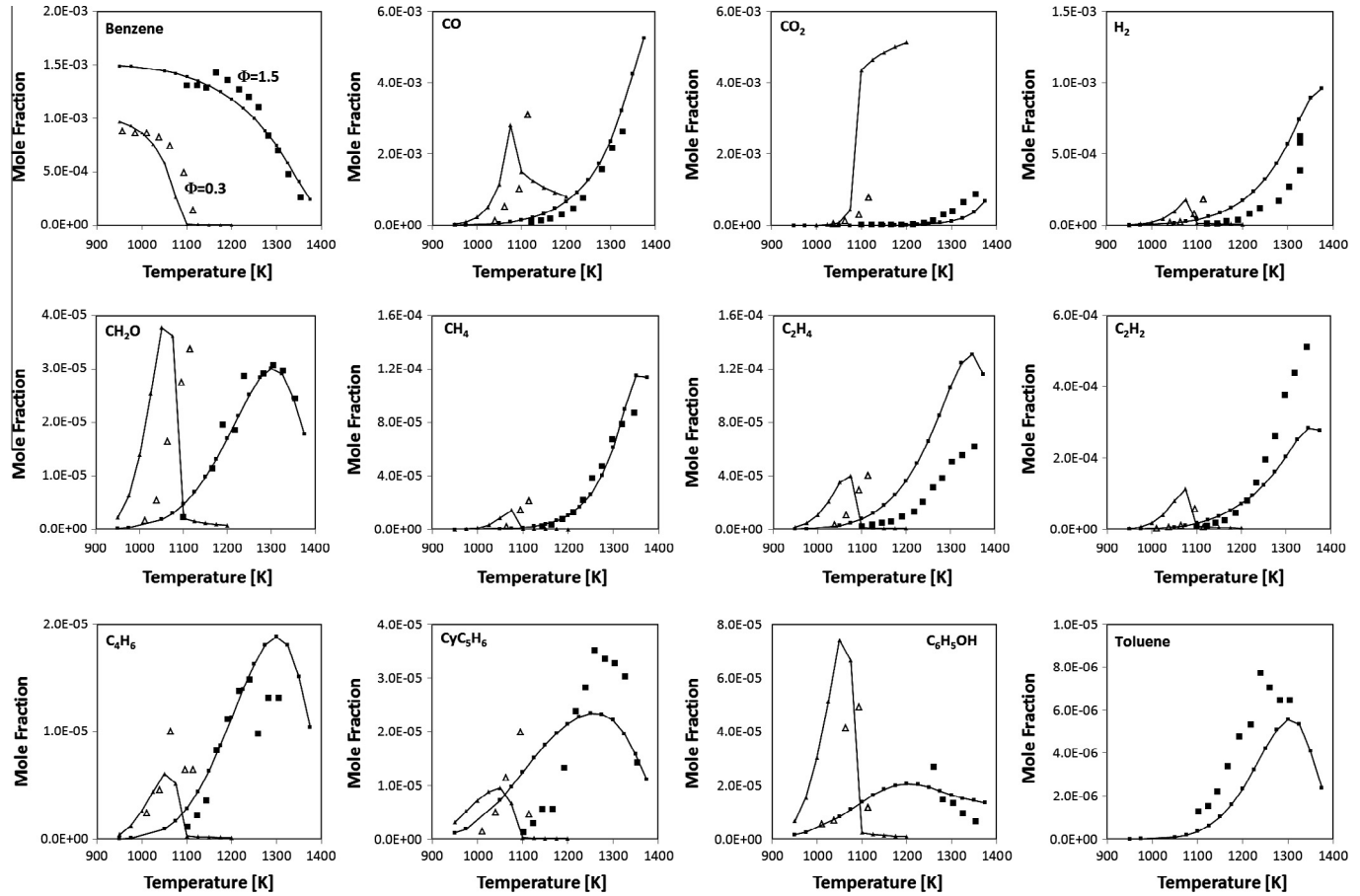


Fig. 11. Benzene oxidation in a jet stirred reactor at $\Phi = 0.3$ (triangles) and $\Phi = 1.5$ (squares), at 1 atm and 0.07 s. Comparisons of experimental (symbols) and predicted (lines) mole fractions [18].

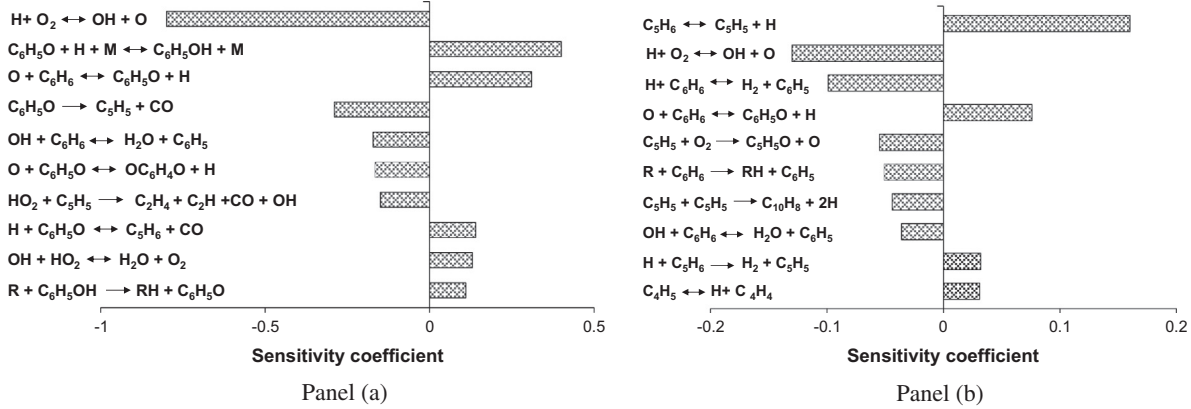


Fig. 12. Sensitivity analysis of benzene at equivalence ratios 0.3 (1050 K and 40% of benzene conversion – panel a) and 1.5 (1200 K and 20% of benzene conversion – panel b).

observed by Metcalfe et al. [11] in low temperature toluene oxidation, where the same chemistry of phenoxy radical plays a crucial role.

3.4.4. Benzene oxidation at 0.46 atm in a micro well-mixed reactor

The kinetic mechanism was also tested and validated on the basis of the experimental data obtained by Chai and Pfefferle [17] using a micro-jet reactor, which approaches a well-stirred reactor under the conditions investigated. The experiments covered the

temperature range 900–1300 K at nominal residence times of ~50 ms and pressures of 350 torr and $\Phi = 0.19$ and $\Phi = 1.02$. Figure 16 presents a comparison between this set of experimental data and model predictions in terms of fuel conversion, CO, CO₂, acetylene, vinyl acetylene, and cyclopentadiene. These data are similar to the data of Ristori et al. [18] at 1 atm and confirm the overprediction of benzene reactivity, mainly in lean conditions. The maximum concentration of cyclopentadiene is overpredicted here, but this is not observed in the Ristori data of Fig. 11.

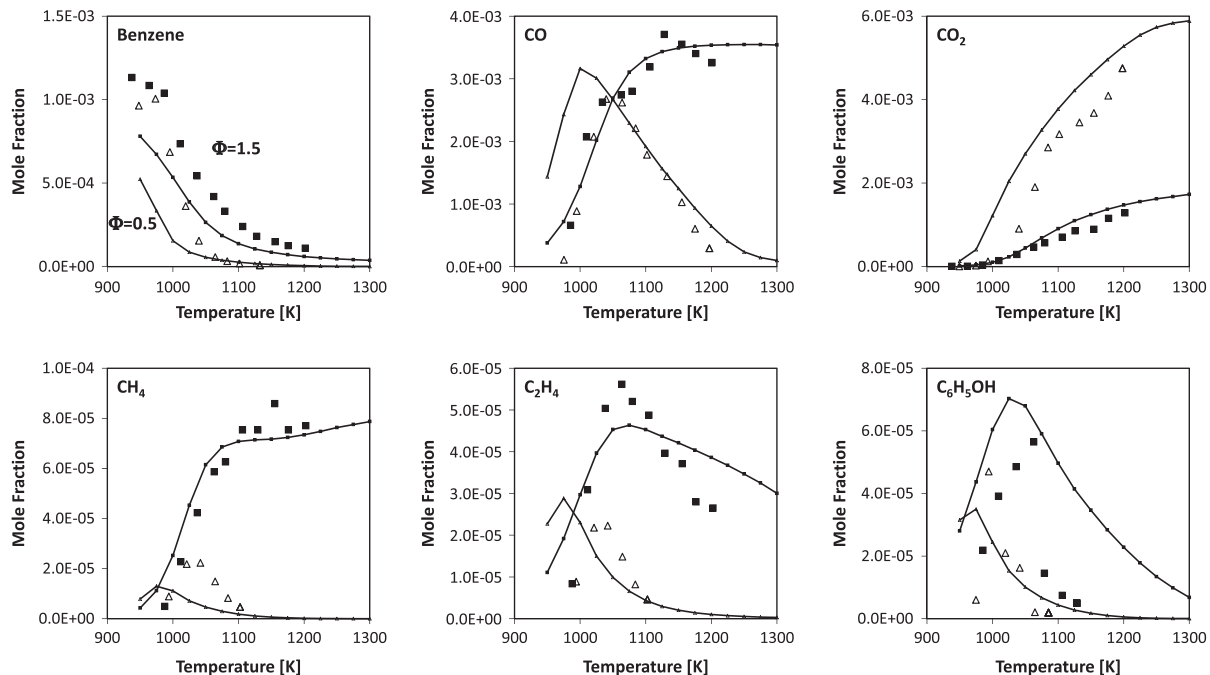


Fig. 13. Benzene oxidation in a jet stirred reactor at $\Phi = 0.5$ (triangles) and $\Phi = 1.5$ (squares), at 10 atm and 0.7 s. Comparisons between experimental (symbols) and predicted (lines with small symbols) mole fractions [16].

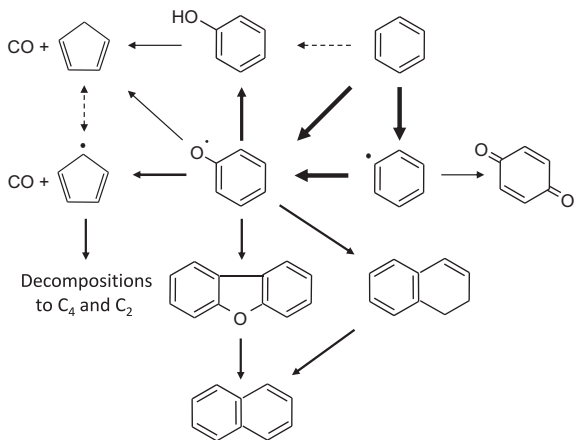


Fig. 14. Major reaction paths of benzene oxidation in a jet stirred reactor at 10 atm and 1000 K. The thickness of the arrows reflects the relative importance of the different reaction paths at $\Phi = 1.5$ and 50% benzene conversion [16].

3.4.5. Low and high temperature oxidation of a mixture benzene-n-decane in a jet stirred reactor

The stoichiometric and atmospheric oxidation of a 75% benzene and 25% n-decane blend was studied by Herbinet et al. [73] in a jet-stirred reactor at temperatures from 500 to 1100 K. A comparison with results obtained with neat n-decane showed that the reactivity of the n-decane is barely affected by the presence of benzene. As it is shown in Fig. 17, model predictions confirm this feature reasonably well. Figure 18 shows detailed comparisons between experimental measurements and model predictions. While several main species confirm that the model's predictions are reasonably good, some deviations can be observed. First and foremost, there are over-predictions of butadiene at low temperatures. These deviations are mainly due to n-decane decomposition and the lumped approach here used. Intermediate unsaturated radicals, generally allyl in type, are supposed to be instantaneously converted into

their β -decomposition products, thus explaining the butadiene over-prediction. Similarly, the acetylene over predictions are mainly due to the successive decomposition reaction of benzoquinone radicals ($C_6H_3O_2$). These deviations could suggest useful extensions of the lumped kinetic scheme, including new intermediate radicals.

3.5. Premixed laminar flames

The combustion chemistry of benzene was also studied in the high temperature conditions typical of flames.

After studying laminar flame speeds, premixed laminar flames at low and atmospheric pressure were analyzed to further validate the mechanism over a wider range of conditions.

3.5.1. Laminar flame speed

Davis and Law [31] reported the laminar speed of benzene/air flames at 298 K and atmospheric pressure. Farrell et al. [74] and Johnston and Farrell [32] determined the laminar flame speeds of benzene at 450 K and 3 atm pressure over a wide range of equivalence ratios, and they also discussed the kinetic factors affecting their values in alkyl substitution of the aromatic ring [9]. More recently, Ji et al. [3] determined the laminar speeds of atmospheric benzene flames at 353 K.

The role of the phenoxy radical is very prominent for benzene flames and is based mainly on the competition between the following reactions:



Phenoxy and the H radical recombine to form phenol, thereby reducing the laminar flame speed, while the reverse occurs for the remaining reactions.

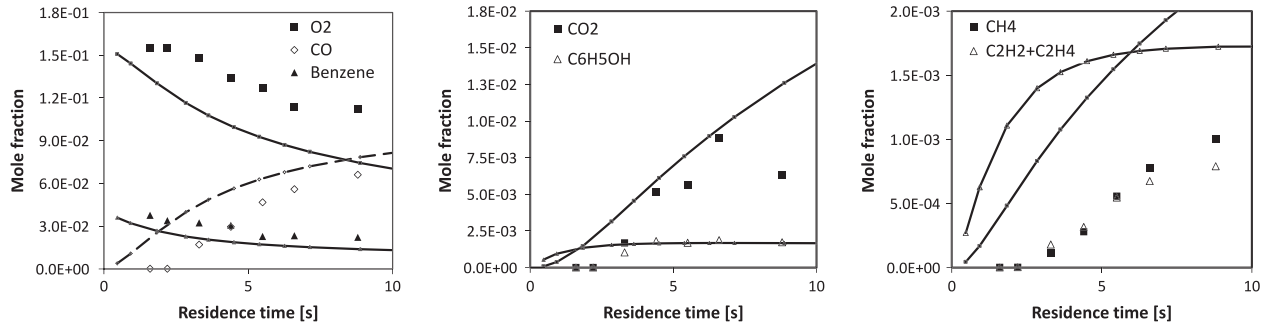


Fig. 15. Benzene oxidation in a jet stirred reactor at 923 K and $\Phi = 1.9$. Experimental (symbols) and predicted mole fractions (lines with small symbols) as a function of residence time [19].

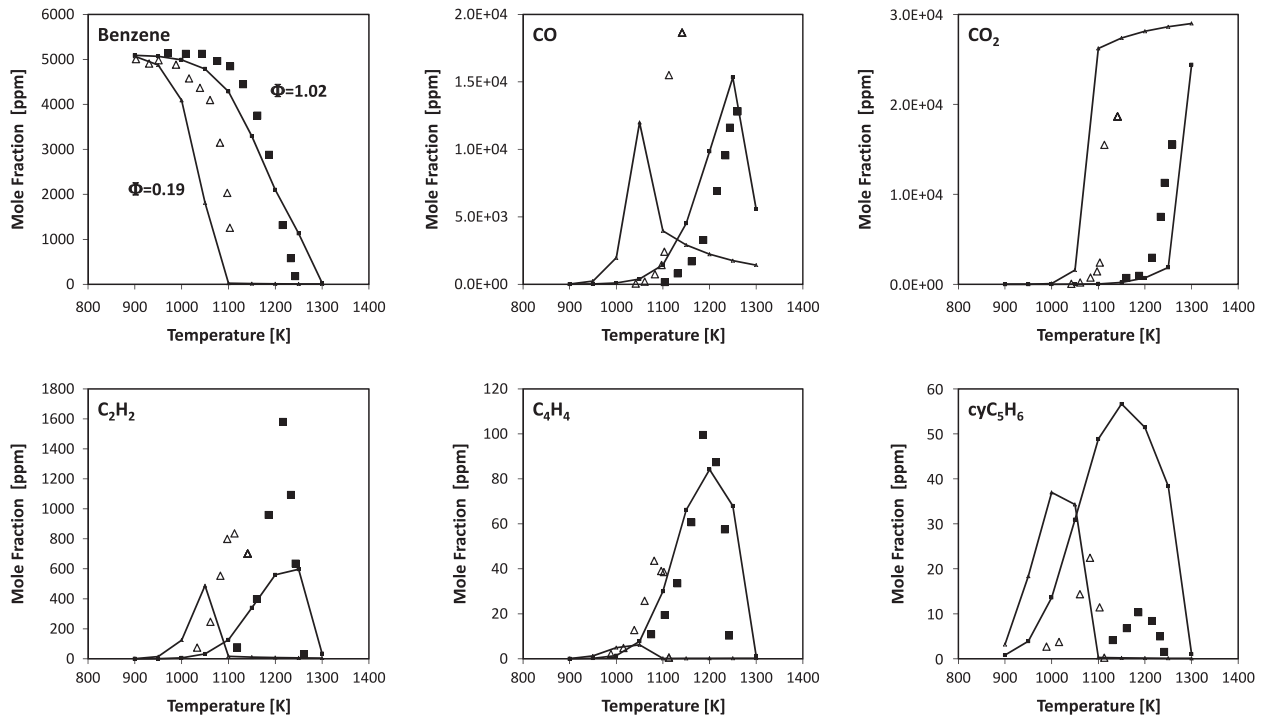


Fig. 16. Benzene oxidation in a jet stirred reactor at $\Phi = 1.02$ (squares) and $\Phi = 0.19$ (triangles), at 350 torr and 50 ms. Comparisons between experimental (symbols) and predicted (lines with small symbols) mole fractions [17].

Figure 19 shows the flame structure of an atmospheric stoichiometric benzene/air flame at $T_0 = 298$ K. As already mentioned in the previous discussion, the role of the phenoxy radical with the formation of phenol in reaction (R29) and benzoquinone in reaction (R31) is very important. Cyclopentadiene is a minor intermediate, while the C_2H_2 profile shows the importance of the parallel and successive decomposition paths. Figure 20 compares experimental and predicted values for the laminar flame speeds of benzene at 1 and 3 atm and different temperatures. The increase in the flame speed at 3 atm observed here is primarily due to the increase of the initial temperature.

As usual, the sensitivity analysis of Fig. 21 shows that benzene premixed laminar flame speed depends mainly on the rate parameters of the C_1 mechanism reactions. Fuel specific reactions are the recombination reactions of H atoms with phenyl to form benzene (R1), with phenoxy to form phenol (R29) and with cyclopentadienyl to form cyclopentadiene. Benzoquinone formations with (R17) and (R31) are also important, both at 1 and 3 atm.

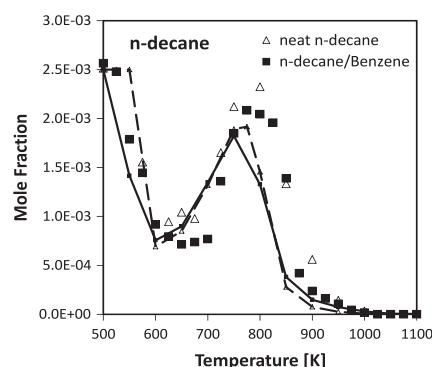


Fig. 17. Effect of benzene on n -decane conversion. Mole fractions of neat n -decane (triangles) and n -decane in the benzene mixture (squares) vs. reactor temperature. Experimental (symbols) and model predictions (lines with small symbols) [73].

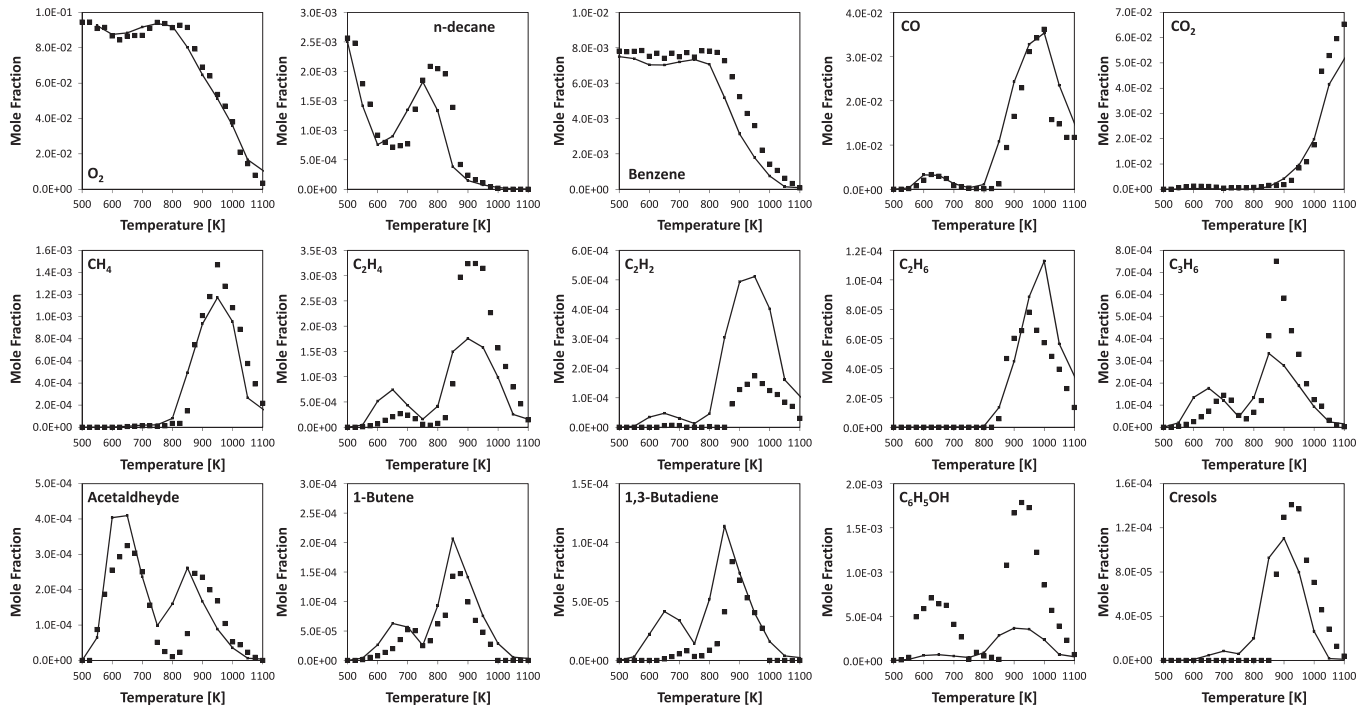


Fig. 18. Mole fractions of relevant species in the oxidation of the benzene/n-decane mixture vs. reactor temperature. Experimental (symbols) and model predictions (lines with small symbols) [73].

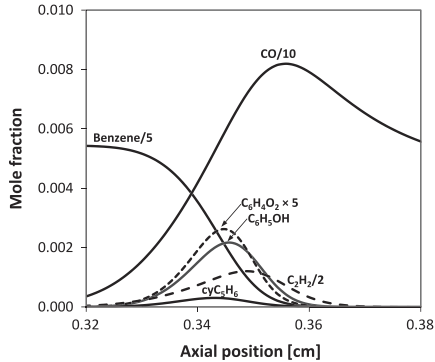


Fig. 19. Flame structure and main reaction paths in atmospheric air-stoichiometric benzene flame at $T_0 = 298$ K.

3.5.2. Low pressure flames

New experimental data relating to low pressure benzene flames in different stoichiometric conditions help further validate the mechanism but high temperature decomposition reactions could be better investigated. Accurate new experimental techniques permit a more comprehensive understanding of the formation and depletion of the intermediate species and radicals in the mixture. Firstly, a set of similar rich flames obtained in three different laboratories is analyzed and compared. Then, the effects of flame stoichiometry and sooting flames are investigated also.

3.5.2.1. Rich low pressure flames. Very similar benzene flames at low pressures (25–40 mbar) with $\Phi = 1.78\text{--}2$ have been studied by many different groups using different experimental techniques [33,35,37,38].

Bittner and Howard [33] studied a near-sooting rich premixed benzene flame at $\Phi = 1.8$ using molecular beam mass spectrometry

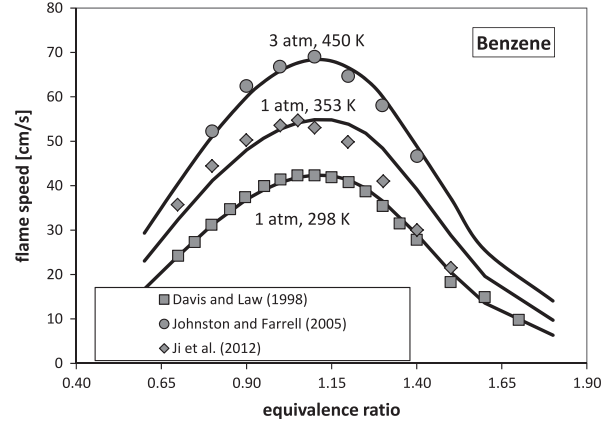


Fig. 20. Benzene laminar flame speed at 1 atm and 298 K (experimental: squares [31]), 1 atm and 353 K (diamonds [3]), and 3 atm and 450 K (circles [32]). Model: solid lines.

(MBMS) and provide much detail regarding detected species. The flame was operating at a total pressure of 26.7 mbar with initial mixture concentration of 13.5% C_6H_6 , 56.5% O_2 , and 30% Ar. A set of comprehensive experimental data from the low pressure pre-mixed $C_6H_6/O_2/Ar$ flame ($\Phi = 1.78$) at 40 mbar was presented by Yang et al. [37] using synchrotron photoionization and MBMS. These data are particularly useful because they provide more detailed isomer identification. Finally, the structure of similar rich flames ($\Phi = 2$) at 45–50 mbar was measured using two different techniques: gas chromatography [38] and MBMS [35].

The experimental conditions of each flame are summarized in Table 4.

These experimental data are very useful not only in further validating the kinetic model but also in evaluating possible uncertainties related to experimental measurements. The aim of this analysis is to compare the main species profiles performed using

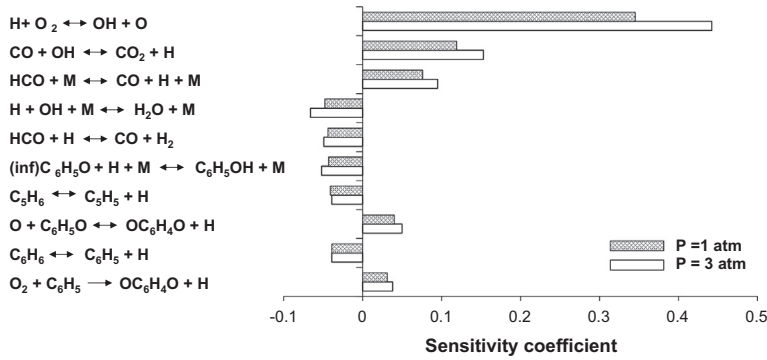


Fig. 21. Sensitivity coefficients of premixed laminar flame speed on reaction rate coefficients for benzene/air flames at 1 and 3 atm and $\Phi = 1.1$.

Table 4
Experimental conditions of the low pressure flames analyzed.

Flame	Temperature (K)	Pressure (atm)	Φ	Composition (mol%)	v (cm/s)	Refs.
A	700–1600	0.0267	1.8	13.5 C ₆ H ₆ /56.5 O ₂ /30 Ar	50	[33]
B	700–1800	0.04	1.78	9.5 C ₆ H ₆ /40.5 O ₂ /50 Ar	32.7	[37]
C	700–1750	0.045	2	12 C ₆ H ₆ /44 O ₂ /44 Ar	40.5	[38]
D	700–1800	0.05	2	11.8 C ₆ H ₆ /44.2 O ₂ /44 Ar	35	[35]

different techniques in order to improve model predictions and to use the model as a tool which may also help analyze experimental discrepancies and uncertainties.

Figure 22 shows the experimental and predicted concentration profiles of major species of the flame of Bittner et al. [33]. Similar flame structures and agreement are also obtained for the remaining flames.

Figures 23–25 show a synoptic view of the comparisons of predicted and experimental mole fraction profiles of the four flames. Flame A and B are reported in the first two columns. Flame C (open symbols and dashed line) and D (filled symbols and solid line) are reported in the third column, because both flames were obtained at Louvain University. The same mole fraction scales for the same species have been adopted to emphasize the differences in the experimental measurements. To better understand the meaning of all the comparisons reported in Figs. 23–25, Fig. 26 reports the rate of production analysis (ROPA) of flame A. Again very similar information is obtained by studying the remaining flames.

The overall consistency of the experimental measurements indicates that these experiments are highly reliable. Similarly, the model predictions agree reasonably well with all the experiments.

At high temperatures and in rich conditions, the most favored decomposition path for benzene is phenyl radical formation with the latter oxidized to form the phenoxy radical. Once again, the phenoxy radical can mostly decompose to cyclopentadiene and CO with reaction (R30) and partly recombine with H atoms to form phenol with reaction (R29).

The following main considerations can be derived from the analysis of these figures:

- Model deviations of C₂ and C₃ species in Fig. 23 are within the experimental uncertainties. Note that C₃H₄ is the sum of allene and propyne and model predictions also agree fairly well with the relative amount of the two isomers, as measured by [38].

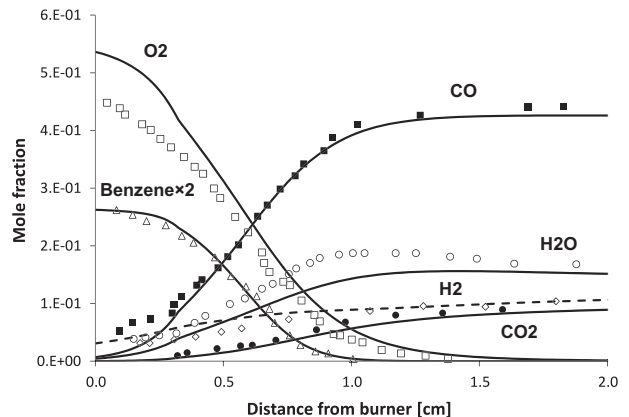


Fig. 22. Experimental and predicted concentration profiles of major species of the flame of Bittner et al. [33].

- C₄H₆ is over-predicted in the flames A and C, while is underpredicted in the flame B. Butadiene is then decomposed mainly producing C₂ and C₄ species.
- C₄H₂ is the most abundant C₄ species and is well predicted by the model. Diacetylene mainly derives from the decomposition of o-C₆H₄:



- Cyclopentadiene is well predicted in flames A and C and under-estimated in flames B and D. The experimental uncertainties seem to be of a similar order of magnitude. The lower concentrations of methylcyclopentadiene are correctly predicted.
- At high temperatures and flame conditions, the H abstraction reactions on the phenyl radical promoted by OH, H and O radicals account for only a small amount of total phenyl depletion. These reactions are taken from Vourliotakis et al. [10] and justify the formation of C₆H₄, with the successive dehydrogenation reactions to form C₆H₃ and then the more stable C₆H₂, which is relatively important with mole fractions up to 10⁻³.
- The mole fractions of phenol, which mainly derives from the very important H recombination reaction of the phenoxy radical (R29), are slightly over predicted in all the flames.
- The predicted formation of heavier aromatics, such as toluene, styrene and phenyl-acetylene is reasonable and consistent compared to the experimental uncertainties, while naphthalene and indene are under-predicted.

3.5.2.2. Low pressure flames and the effect of stoichiometry. Detilleux et al. [38] also investigated the influence of flame stoichiometry

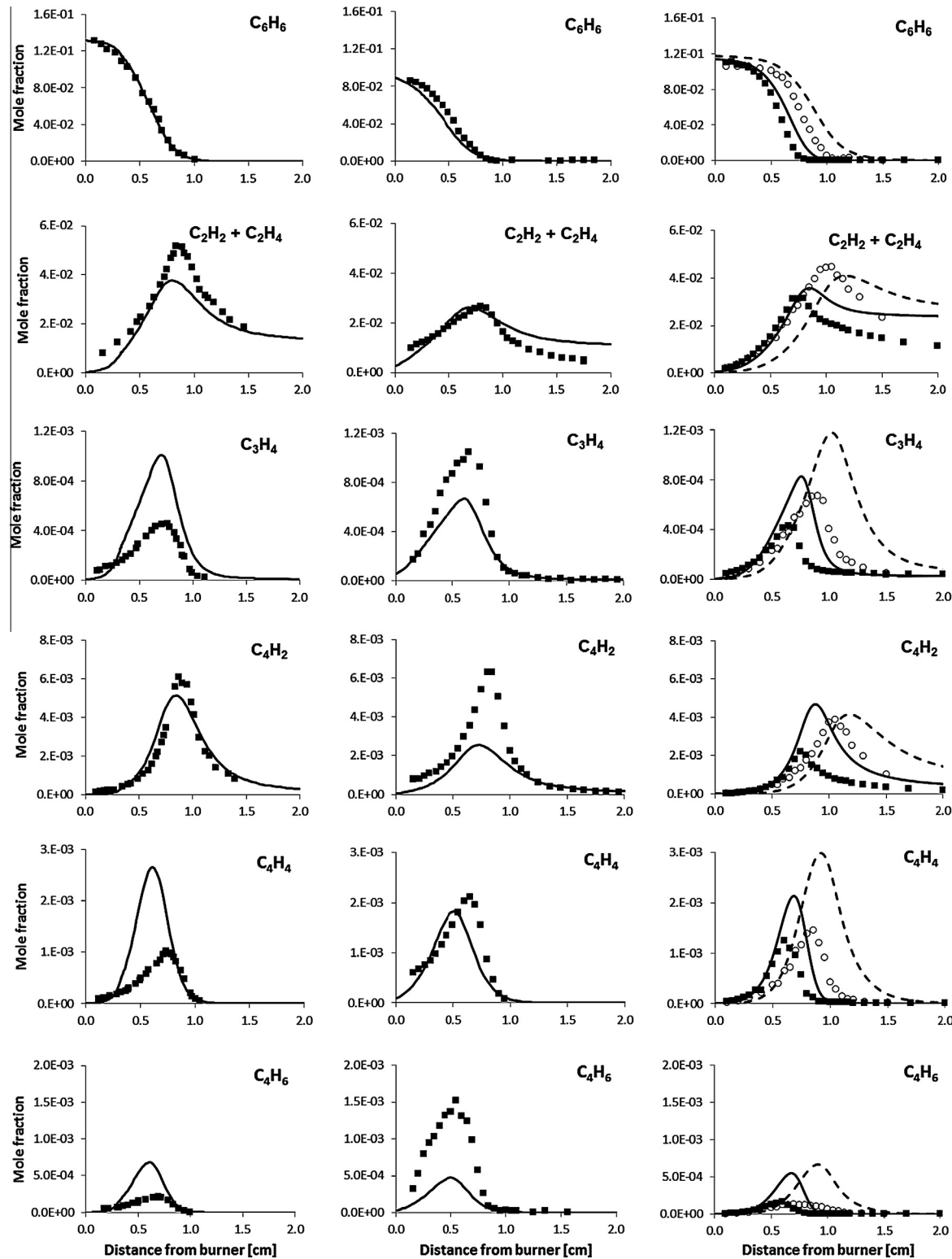


Fig. 23. Profiles of benzene and major C_2 , C_3 , C_4 combustion products in rich flames. First column: flame A; second column: flame B; third column: flames C and D. Experimental: symbols. Model predictions: lines. Flame conditions are reported in Table 4.

($\Phi = 0.7$, 1, and 2). Relevant comparisons between predictions and experimental measurements of the major species of benzene combustion in lean ($\Phi = 0.7$) and rich conditions ($\Phi = 2$) are reported in the Fig. 27. The flame structure is well predicted in lean conditions, while in stoichiometric and rich conditions, there is a small time

delay in the predicted species profiles, as already observed in Fig. 23.

According to the rate of production analysis, the decomposition path of benzene to form phenoxy directly with reaction (R9) in rich conditions accounts for 15%, while in lean condi-

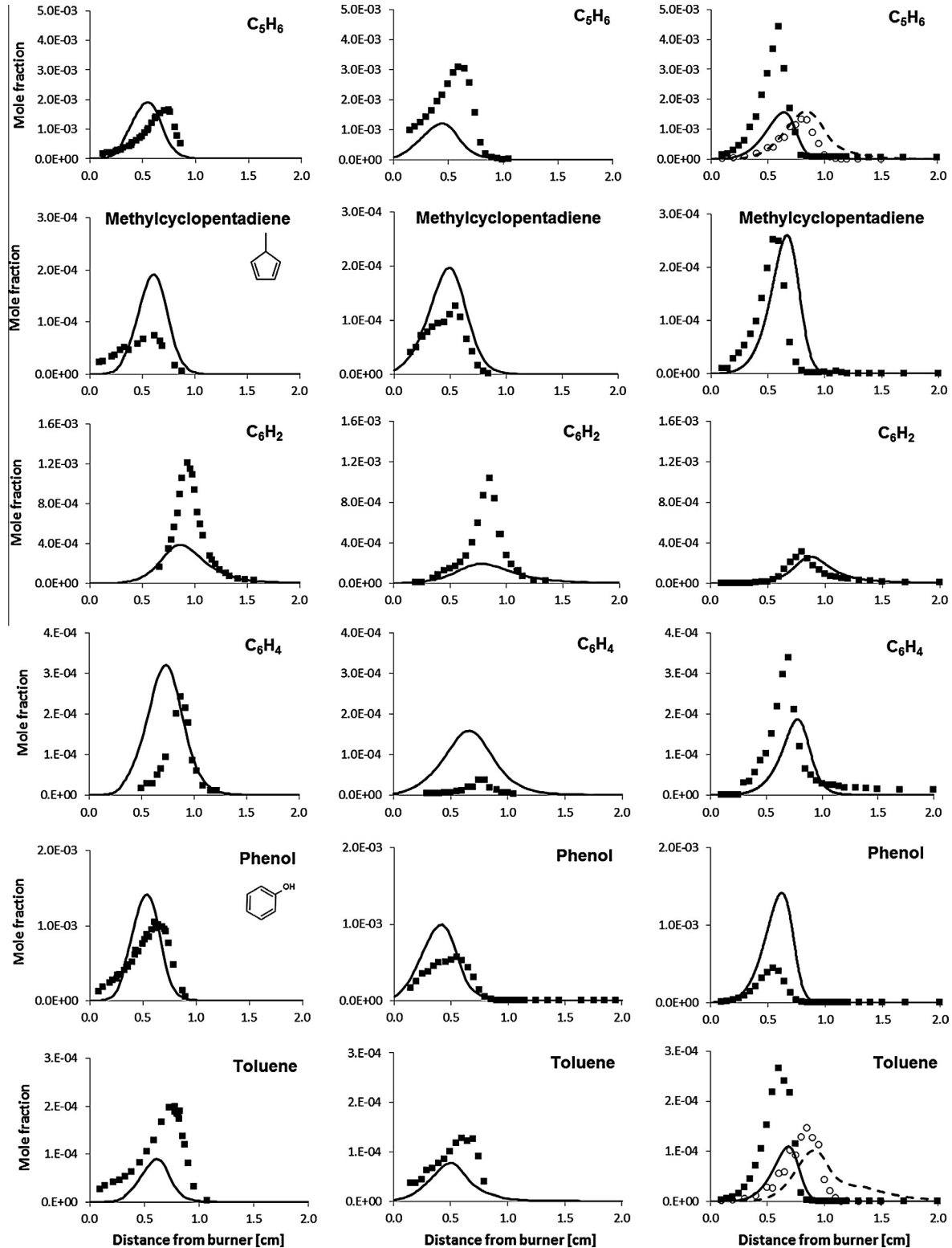


Fig. 24. Profiles of the major C₅, C₆ and C₇ products of benzene combustion in rich flames. First column: flame A; second column: flame B; third column: flame C and D. Experimental: symbols. Model predictions: lines. Flame conditions are reported in Table 4.

tions, this route accounts for 30% of benzene decomposition. The C₂ species profile is correctly predicted in all the flames, whereas in rich conditions, there is a partial lack of acetylene decomposition in the post-flame zone. Cyclopentadiene is well estimated and is one of the main species responsible for C₄ and C₃ forma-

tion. As observed earlier, there is a systematic over-prediction of butadiene in these flames too. Lastly, toluene agrees quite well in both conditions and derives mainly from the recombination of phenyl and methyl radicals as well as from the H and benzyl (C₇H₇) recombination reaction.

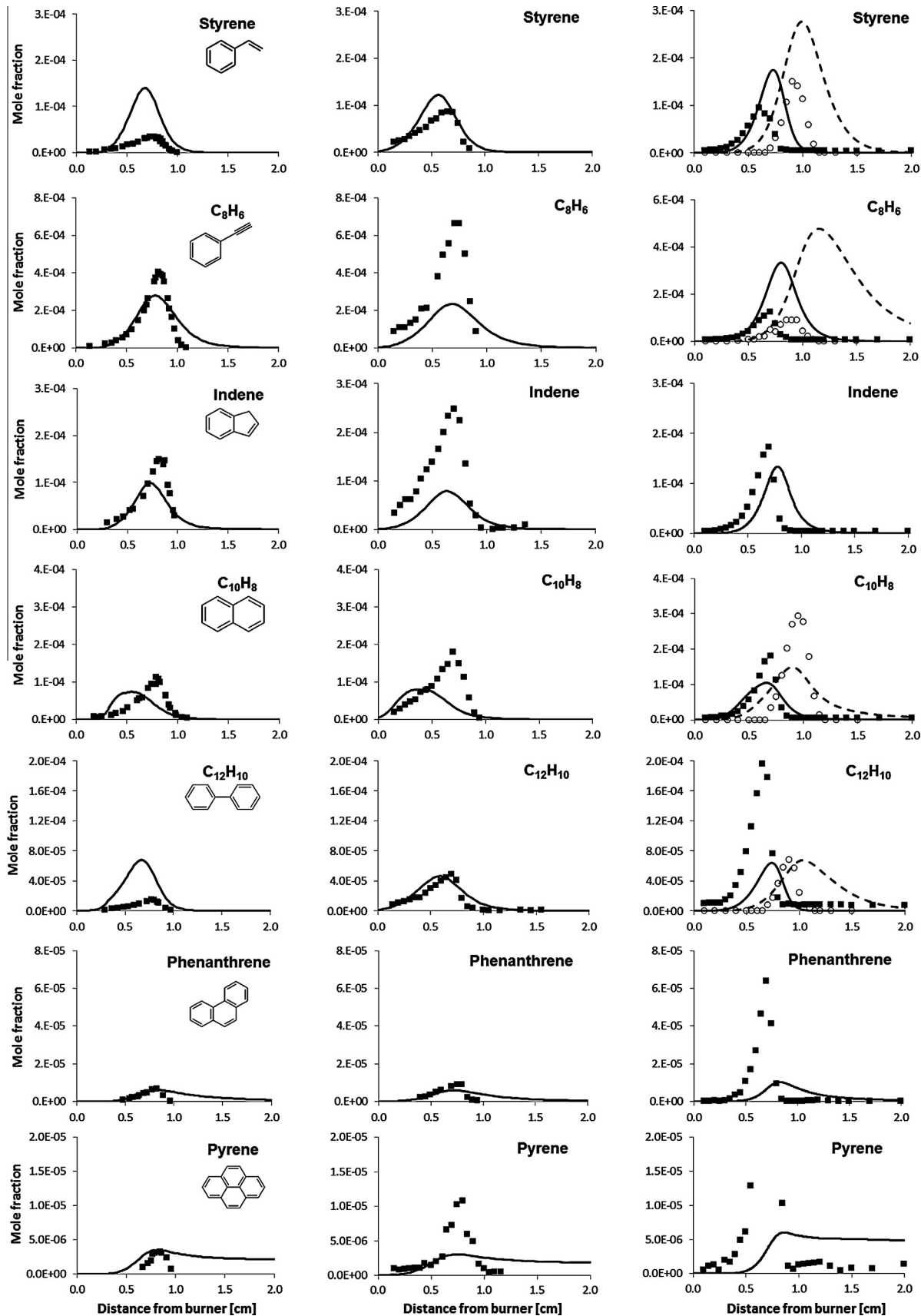


Fig. 25. Profiles of the heavier species of benzene combustion in rich flames. First column: flame A; second column: flame B; third column: flame C and D. Experimental: symbols. Model predictions: lines. Flame conditions are reported in Table 4.

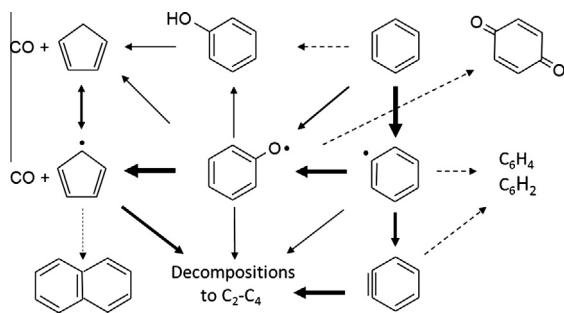


Fig. 26. Main reaction pathways in flame A [33]. The thickness of the arrows reflects the relative importance of the different reaction paths.

3.5.3. Rich atmospheric flames

Two sets of experimental data relating to atmospheric benzene flames investigate the effect of flame temperature and flame stoichiometry.

Tregrossi et al. [34] studied premixed fuel-rich benzene/air flames at atmospheric pressure and with different C/O ratios (0.72–0.77). Recently, these flames were also analyzed at fixed mixture composition (C/O = 0.8) and under different temperature conditions ($T_{\max} = 1720$ K and 1810 K) by Russo et al. [39]. These sooting flames offer a better understanding of the evolution of heavier species, such as polycyclic aromatic hydrocarbons (PAH), which are precursors of soot formation. Figures 28 and 29 show the comparison between experimental and predicted mole fraction profiles for the relevant detected species in the flames with C/O ratios 0.72 and 0.77. These figures show that the structure of the flame and the final and intermediate C₂–C₃ species are well predicted, while the methane maximum is partially underestimated in both flames. It is also worth observing that methane peak was overestimated by a factor of two in the low pressure flame C of Table 4, as shown in Fig. 30. In atmospheric flames, butadiene and naphthalene are significantly and systematically over-predicted, while cyclopentadiene agrees well with the experimental data. Minor over-predictions of phenol and indene are also observed. Peak concentrations of biphenyl, phenanthrene and pyrene are also over-predicted. Similar deviations and comments can be also drawn from the comparisons with the atmospheric flames of Russo et al. [39], which investigate the temperature effect on soot formation. The over-predictions of heavy species could be at least partially reduced by introducing the kinetic model for soot

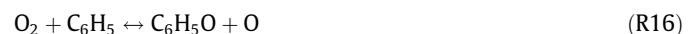
formation [54]. This kinetic mechanism moves the PAH towards heavier species contributing to a possible reduction of these discrepancies. Of course, the soot formation mechanism deserves detailed discussion, but this is beyond the remit of this paper.

4. Final comments and conclusions

The comparative analysis of Figs. 8, 14 and 26, which show the main reaction paths of benzene decomposition, provides a better description of the overall benzene oxidation mechanism in the different reacting systems. The addition reaction of O atoms to benzene to form phenoxy radicals (R9) always competes with the H abstraction reactions, because it is difficult to remove H atoms from the aromatic ring. H (R2) and OH (R3) are the major H abstracting radicals and the relative prevailing role of (R2) is mainly seen in flame conditions, due to the back diffusion of H atoms. The H abstraction reaction of O atoms:



accounts for less than 10% of the total H abstraction reactions on benzene, and is also of limited importance with respect to the O addition to form phenoxy (R9). Phenyl radical addition to O₂ to form phenoxy radical:



always prevails with respect to benzoquinone formation (R17). Nonetheless, (R17) and (R31) are sensitive reactions in premixed laminar flame speed computations.

Thus, benzene decomposition mostly moves through the successive reactions of the phenoxy radical which assumes a central role in the overall oxidation mechanism. In the high or intermediate temperatures of benzene oxidation in the flames (Fig. 26) or in the flow reactor (Fig. 8), the phenoxy radical mainly decomposes to form cyclopentadienyl radical (R28). The recombination reaction with H to form phenol (R29) is less significant. Decomposition reactions of the phenoxy radical with the breaking of the aromatic ring to form C₂–C₄ species play a marginal role, also in flame conditions. At high temperatures, the C₅H₅ radical mainly decomposes to form C₄ and lower species.

The main reaction paths of benzene decomposition from Fig. 14 show that, at high pressure and lower temperatures, phenoxy radical decomposition is less important and recombination reaction to form dibenzofuran (R40) plays an increasingly important role. A

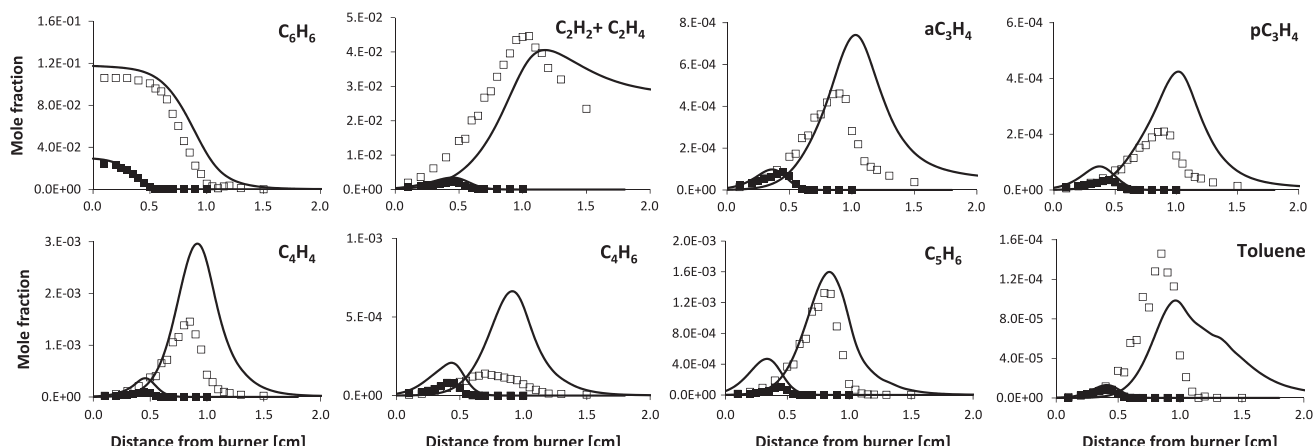


Fig. 27. Mole fraction profiles of benzene and intermediate species in low pressure benzene flames. Experiments ($\phi = 2$: open squares; $\phi = 0.7$: solid squares) and predictions (lines) [38].

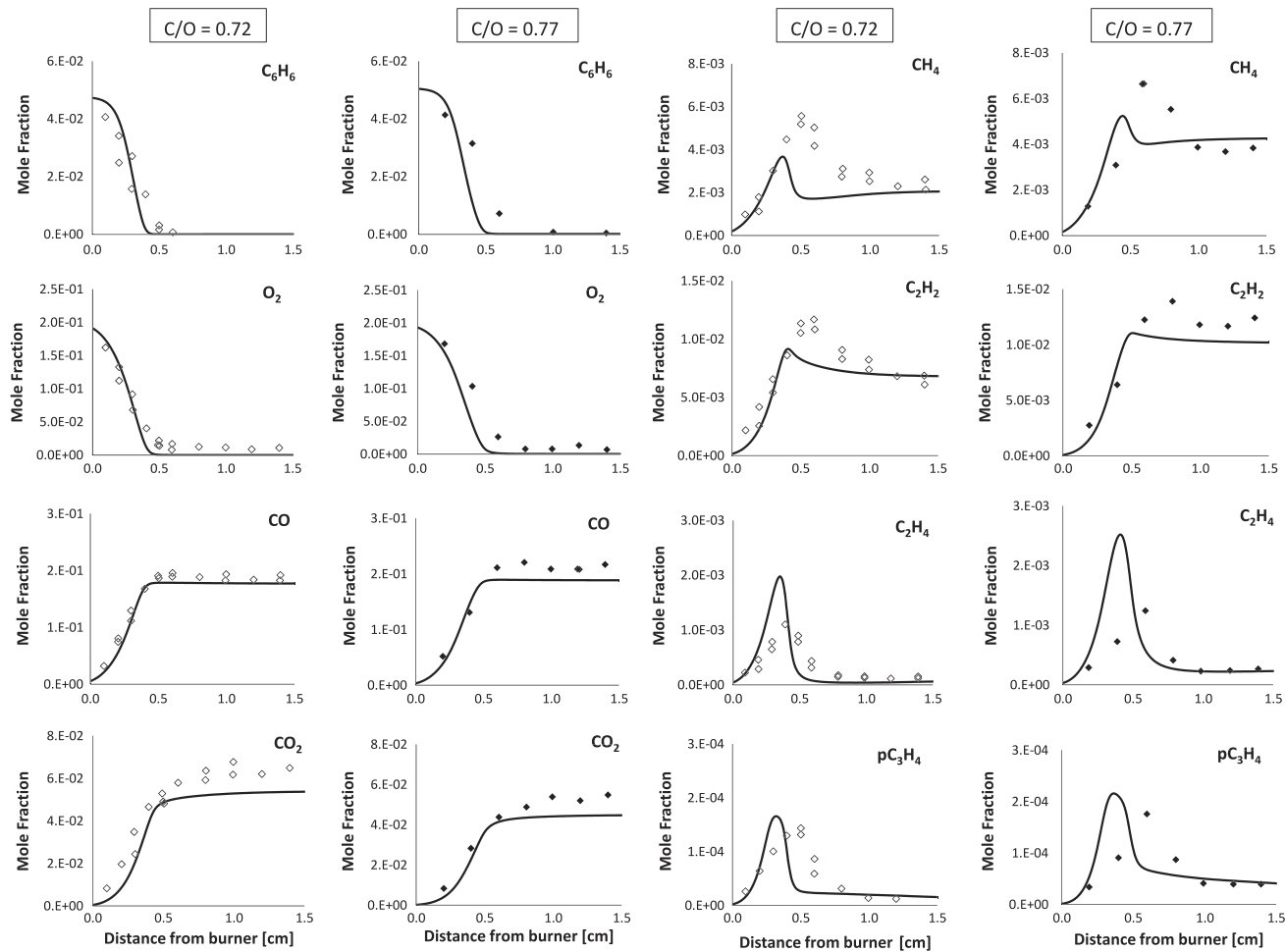


Fig. 28. Mole fraction of important species of rich benzene atmospheric flames. Experimental data (open diamonds: C/O = 0.72; filled diamonds: C/O = 0.77) and model predictions (lines) [34].

similar consideration also applies to C₅H₅ radicals and to their recombination reaction.

As shown in Figs. 2–6, temperature strongly affects benzene pyrolysis. At lower temperatures, recombination reactions are favored and a significant amount of biphenyl is formed with (R21) and (R22). Increasing the temperature, phenyl radical can also break the aromatic ring and form C₂ and C₄ species. At high temperatures, the acetylene addition on the aromatic ring forms PAHs through the typical HACA mechanism [53], starting from phenyl-acetylene. At very high temperatures ($T > 1800$ K), the aromatic ring decomposition starts to compete and prevail on PAHs formation. This pyrolysis mechanism explains the well known bell shaped temperature dependence of the soot volume fraction [75] and confirms the importance of benzene as intermediate in soot formation. Although the soot formation is not the focus of the present study, it is worth referring to some important review articles [2,76–78].

In conclusion, the benzene decomposition mechanism was systematically and hierarchically revised by moving from pyrolysis experiments to partial oxidation and combustion in very lean conditions. A wide range of temperatures and pressures was analyzed and the predictions of a general kinetic model were compared with a large set of experimental measurements coming from different sources. The overall agreement was satisfactory, even if the benzene reactivity was over-predicted at low temperatures in the JSR reactors.

The comparative analysis and synoptic view of the similar low pressure flames (Figs. 23–25) as well the shock tube experiments reported in Fig. 10, not only allow a more reliable validation of the kinetic scheme but also show the possible use of the kinetic scheme as a tool for unifying measurements and indicating areas of major experimental uncertainties.

The significant interactions between benzene, phenol and cyclopentadiene (together with phenyl, phenoxy and cyclopentadienyl radicals) emphasize the need for combined validation of the pyrolysis and oxidation mechanism of these three fuels. While cyclopentadiene pyrolysis and combustion was the object of a recent work [12], comparisons between model predictions and experimental data relating to phenol pyrolysis, hydropyrolysis and oxidation are reported in the Appendix A.

Acknowledgments

The authors gratefully acknowledge the Reviewers for their useful comments, Dr. P. Dagaut in making the data of the Orléans JSR available, Prof. J. Vandooren and V. Dias for benzene flames data, and Dr. A. Ciajolo and C. Russo for the atmospheric sooting flame data.

This work was partially supported by the PRIN 2008 Project: “Cinetica dettagliata di formazione di idrocarburi poliaromatici e nanoparticelle da processi di combustione”.

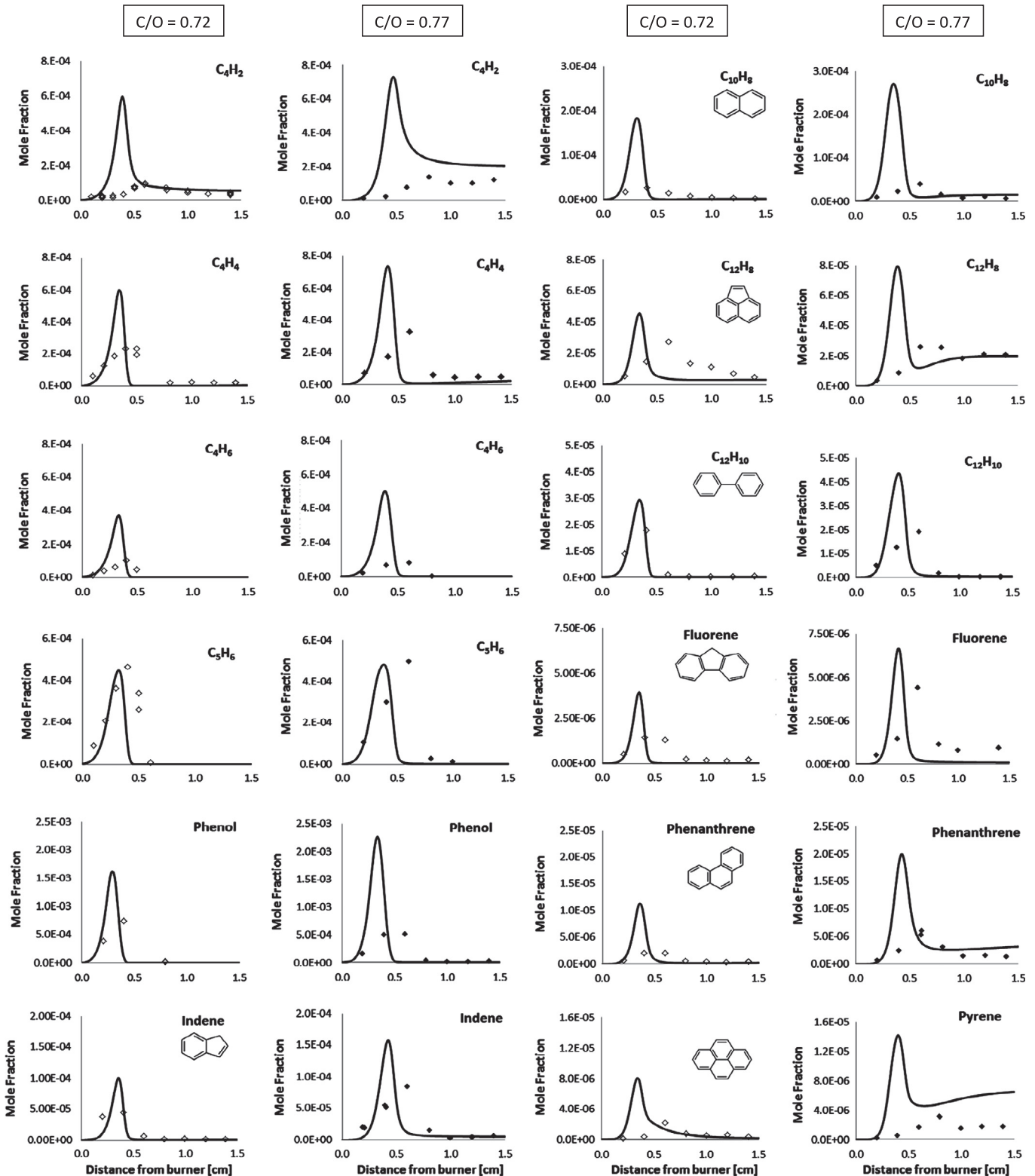


Fig. 29. C_4 and heavier species of two rich benzene atmospheric flames. Experimental data (open diamonds: $\text{C}/\text{O} = 0.72$; filled diamonds: $\text{C}/\text{O} = 0.77$) and model predictions [34].

Appendix A

A.1. Pyrolysis and oxidation of phenol in the Princeton flow reactor

Phenols are common chemicals and notable intermediates in aromatic combustion. They also deserve special attention as possi-

ble precursors of dibenzofuran. The pyrolysis of phenol, previously studied by Lovell et al. [69], was extended to oxidation conditions by Brezinsky et al. [15]. Consistent with prior findings, CO, cyclopentadiene, and benzene were main reaction intermediates, together with acetylene, benzene, 1,3-butadiene, ethene, and methane. It is well defined that CO formation mainly occurs via a

molecular elimination reaction after isomerization of phenol to a cyclohexadienone intermediate [15].

Figure A1 shows a comparison between experimental measurements and model predictions for the mole fraction profiles of acetylene, cyclopentadiene, butadiene and benzene in the Princeton Plug Flow Reactor [15]. These comparisons refer to the pyrolysis and oxidation ($\Phi = 1.73$ and $\Phi = 0.64$) of phenol at about 1170 K.

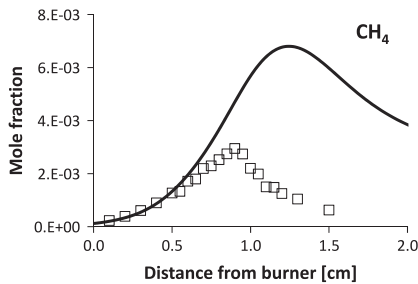


Fig. 30. CH_4 profile in low pressure and rich benzene flame. Experiments: symbols and model predictions: line [38].

A.2. Oxidation of phenol in the Lyngby flow reactor

In their kinetic study on benzene pyrolysis and oxidation, Alzuetta et al. [14] also performed separate experiments to study the phenol pyrolysis and oxidation in the temperature range 900–1450 K. Figure A2 shows a comparison between experimental data and model predictions of CO and CO_2 during the oxidation of 28 ppm of phenol in very lean conditions as a function of reactor temperature.

A.3. Thermolysis of 0.6–6 vol.% phenol in H_2 at atmospheric pressure between 922 and 1175 K

Manion and Louw [13] analyzed the thermolysis of 0.6–6 vol.% phenol in H_2 at atmospheric pressure between 922 and 1175 K. They observed and confirmed the presence of the two main overall reactions, which yield benzene and CO respectively. Secondary products include methane, acetylene, ethylene, ethane, naphthalene, indene, and small amounts of other hydrocarbons; these products appear to stem mainly from the C5 species. Thus, naphthalene and indene typically arise from the recombination of two cyclopentadienyl radicals and from the cycloaddition reactions of

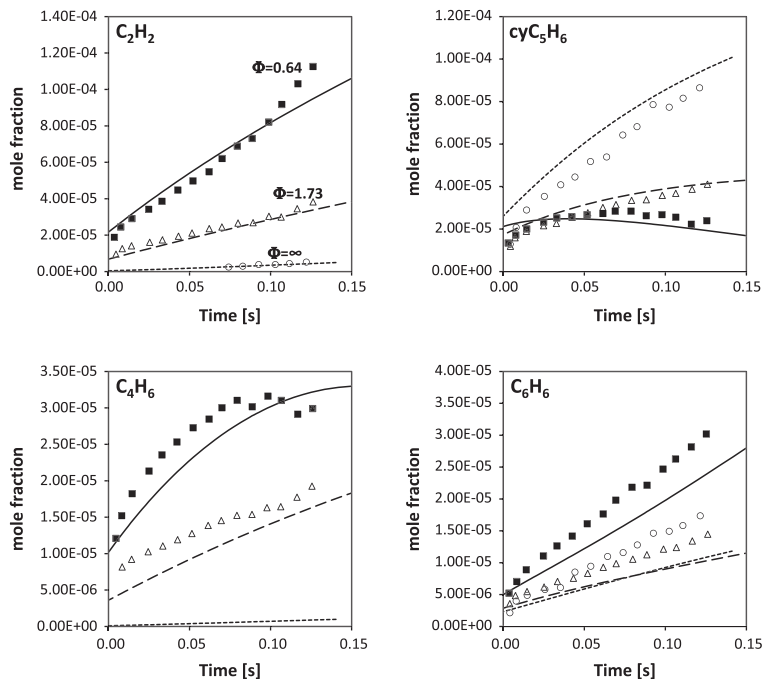


Fig. A1. Acetylene, cyclopentadiene, butadiene and benzene profiles from the pyrolysis and oxidation of phenol at ~1170 K in the Princeton plug flow reactor [15]. Experimental data (533 ppm fuel and $\Phi = 0.64$: squares; $\Phi = 1.73$: triangles; 1004 ppm fuel and pyrolysis conditions: circles), model predictions (lines with small symbols). Butadiene was not detected in pyrolysis conditions.

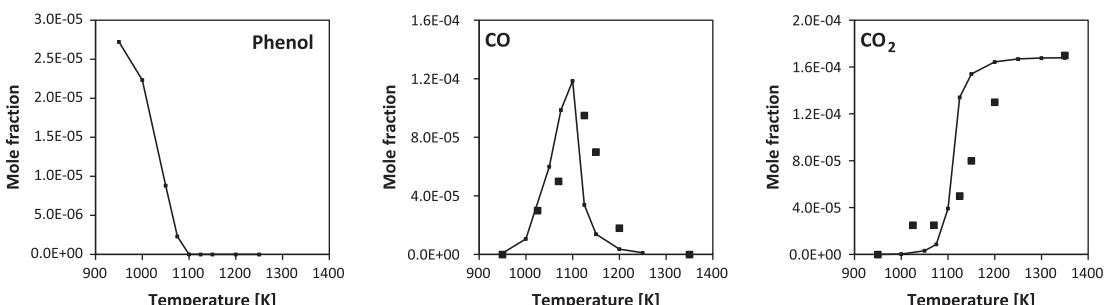


Fig. A2. Comparison between experimental data and model predictions for CO and CO_2 during oxidation of 28 ppm of phenol at $\lambda = 1275$ as function of temperature [14].

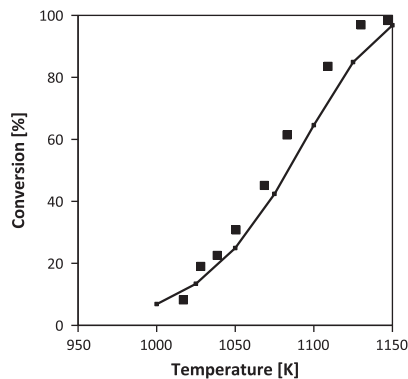


Fig. A3. Conversion of phenol vs. temperature in the thermolysis of phenol/H₂ mixtures [13]. Experimental data (symbols) and model predictions (lines).

these radicals with cyclopentadiene molecules [12]. Manion and Louw also observed dibenzofuran (C₁₂H₈O), which was never present in amounts greater than 0.06 mol% of the phenol introduced. The recombination of phenoxy radicals with H₂O elimination (R40) is able to explain the dibenzofuran formation [60].

Figure A3 reports the phenol conversion vs. reactor temperature at 3 s, while **Figure A4** shows the comparison of the corresponding model predictions with the experimental data in terms of carbon selectivity of major and minor products (C% selectivity = C in products/Converted C × 100). The overall agreement, both in terms of conversion and selectivities of the different products, is satisfactory and it shows the reliability of the phenol mechanism in this reacting environment also.

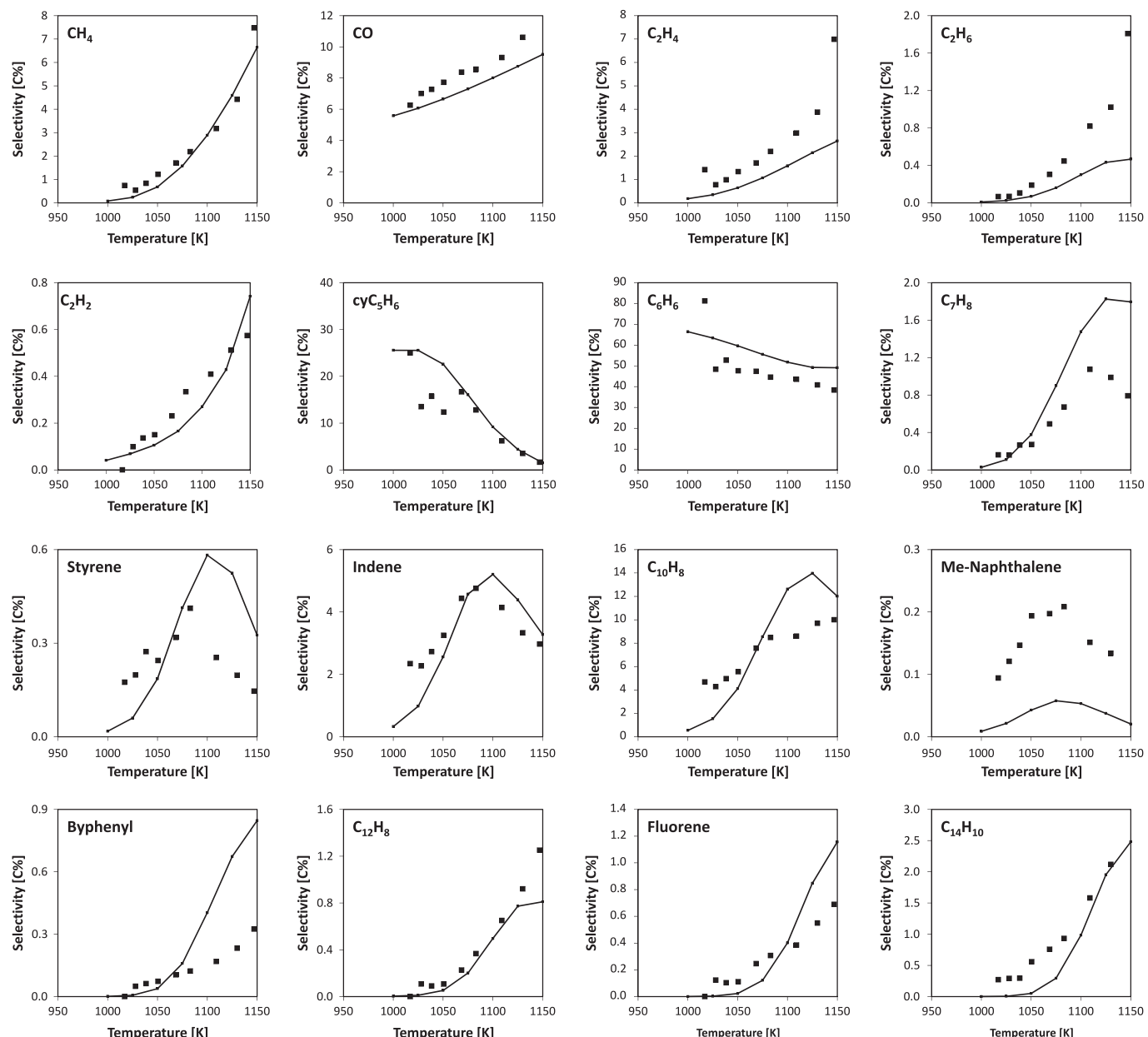


Fig. A4. C% selectivity of main and minor products in the thermolysis of phenol/H₂ mixtures. Experimental data (symbols) and model predictions (lines) [13].

References

- [1] K. Narayanaswamy, G. Blanquart, H. Pitsch, *Combust. Flame* 157 (2010) 1879–1898.
- [2] H. Wang, *Proc. Combust. Inst.* 33 (2011) 41–67.
- [3] C. Ji, E. Dames, H. Wang, F.N. Egolfopoulos, *Combust. Flame* 159 (2012) 1070–1081.
- [4] A.S. Violi, S. Yan, E.G. Eddings, A.F. Sarofim, S. Granata, T. Faravelli, E. Ranzi, *Combust. Sci. Technol.* 174 (2002) 399–417.
- [5] M.B. Colket, J.T. Edwards, S. Williams, N.P. Cernansky, D.L. Miller, F.N. Egolfopoulos, P. Lindstedt, K. Seshadri, F.L. Dryer, C.K. Law, D.G. Friend, D.B. Lenhart, H. Pitsch, A. Sarofim, M. Smooke, W. Tsang, *AIAA Paper AIAA-2007-0770*, 2007.
- [6] K. Brezinsky, *Prog. Energy Combust. Sci.* 12 (1) (1986) 1–24.
- [7] J.L. Emdee, K. Brezinsky, I. Glassman, *J. Phys. Chem.* 96 (5) (1992) 2151–2161.
- [8] E. Ranzi, A. Sogaro, P. Gaffuri, G. Pennati, C.K. Westbrook, W.J. Pitz, *Combust. Flame* 99 (2) (1994) 201–211.
- [9] E. Ranzi, A. Frassoldati, R. Grana, A. Cuoci, T. Faravelli, A.P. Kelley, C.K. Law, *Prog. Energy Combust. Sci.* 38 (4) (2012) 468–501.
- [10] G. Vourliotakis, G. Skevis, M.A. Founti, *Energy Fuels* 25 (2011) 1950–1963.
- [11] W.K. Metcalfe, S. Dooley, F.L. Dryer, *Energy Fuels* 25 (11) (2011) 4915–4936.
- [12] C. Cavallotti, D. Polino, A. Frassoldati, E. Ranzi, *J. Phys. Chem. A* 116 (13) (2012) 3313–3324.
- [13] J.A. Manion, R. Louw, *J. Phys. Chem.* 93 (9) (1989) 3563–3574.
- [14] M.U. Alzueta, P. Glarborg, K. Dam-Johansen, *Int. J. Chem. Kinet.* 32 (2000) 498–522.
- [15] K. Brezinsky, M. Pecullan, I. Glassman, *J. Phys. Chem. A* 102 (1998) 8614–8619.
- [16] A. Marchal, M. Cathonnet, P. Dagaut, M. Reuillon, M. Audinet, G. Belot, J.-F. Béziau, Proceedings of the Joint Meeting of the French and German Sections of the Combustion Institute, Mulhouse, October 1995, pp. 11–13.
- [17] Y. Chai, L.D. Pfefferle, *Fuel* 77 (4) (1998) 313–320.
- [18] A. Ristori, P. Dagaut, A. El Bakali, G. Pengloan, M. Cathonnet, *Combust. Sci. Technol.* 167 (1) (2001) 223–256.
- [19] I. Da Costa, R. Fournet, F. Billaud, F. Battin-Leclerc, *Int. J. Chem. Kinet.* 35 (10) (2003) 503–524.
- [20] C. Venkat, K. Brezinsky, I. Glassman, *Proc. Combust. Inst.* 19 (1982) 143–152.
- [21] A.B. Lovell, K. Brezinsky, I. Glassman, *Proc. Combust. Inst.* 22 (1988) 1063–1074.
- [22] A. Schöbel-Ostertag, M. Braun-Unkhoff, C. Wahl, L. Krebs, *Combust. Flame* 140 (2005) 359–370.
- [23] R.D. Kern, C.H. Wu, G.B. Skinner, V.S. Rao, J.H. Kiefer, J.A. Towers, L.J. Mizerka, et al., *Proc. Combust. Inst.* 20 (1984) 789–797.
- [24] A. Burcat, C. Snyder, T. Brabbs, Ignition Delay Times of Benzene and Toluene with Oxygen in Argon Mixtures, NASA Technical Memorandum 87312, May 1986.
- [25] K. Thyagarajan, K.A. Bhaskaran, *Int. J. Energy Res.* 15 (1991) 235–248.
- [26] K. Fieweger, R. Blumenthal, G. Adomeit, *Proc. Combust. Inst.* 25 (1994) 1579–1585.
- [27] A. Laskin, A. Lifshitz, *Proc. Combust. Inst.* 26 (1996) 669–677.
- [28] R. Sivaramakrishnan, K. Brezinsky, H. Vasudevan, R.S. Tranter, *Combust. Sci. Technol.* 178 (2006) 285–305.
- [29] G. Mittal, C.-J. Sung, *Combust. Flame* 150 (2007) 355–368.
- [30] R.R. Baldwin, M. Scott, R.W. Walker, *Proc. Combust. Inst.* 21 (1) (1988) 991–1000.
- [31] S.G. Davis, C.K. Law, *Combust. Sci. Technol.* 140 (1998) 427–449.
- [32] R.J. Johnston, J.T. Farrell, *Proc. Combust. Inst.* 30 (2005) 217–224.
- [33] J.D. Bittner, J.B. Howard, *Proc. Combust. Inst.* 28 (1981) 1105–1116.
- [34] A. Tregrossi, A. Ciajolo, R. Barbella, *Combust. Flame* 117 (1999) 553–561.
- [35] F. Defoex, V. Dias, C. Renard, P.J. VanTiggelen, J. Vandooren, *Proc. Combust. Inst.* 30 (2005) 1407–1415.
- [36] A. El Bakali, M. Ribaucour, A. Saylam, G. Vanhove, E. Therssen, J.F. Pauwels, *Fuel* 85 (2006) 881–895.
- [37] B. Yang, Y. Li, L. Wei, C. Huang, J. Wang, Z. Tian, R. Yang, L. Sheng, Y. Zhang, F. Qi, *Proc. Combust. Inst.* 31 (2007) 555–563.
- [38] V. Detilleux, J. Vandooren, *Combust. Expl. Shock Waves* 45 (2009) 392–403.
- [39] C. Russo, F. Stanzione, A. Tregrossi, M. Alfè, A. Ciajolo, *Combust. Flame* 159 (2012) 2233–2242.
- [40] T. Faravelli, F. Giovannini, D. Rivellini, E. Ranzi, A. D'Anna, A. Ciajolo, Kinetic Modeling of New Formulated Gasoline, III International Conference ICE 97–Internal Combustion Engine: Experiments and Modeling, Capri, September 169, 1997, pp. 17–19.
- [41] R.J. Kee, F. Rupley, J.A. Miller, *Chemkin II: A Fortran Chemical Kinetics Package for the Analysis of Gas-phase Chemical Kinetics*, Sandia Report SAND89-8009, Sandia National Laboratories, 1989.
- [42] E. Goos, A. Burcat, B. Rusic, Third Millennium Thermodynamic Database for Combustion and Air-Pollution Use, with Updates from Active Thermochemical Tables, 2010, <<http://garfield.chem.elte.hu/burcat/BURCAT.THR>>.
- [43] S.W. Benson, *Thermochemical Kinetics*, second ed., Wiley, New York, 1976.
- [44] D. Manca, G. Buzzi Ferraris, T. Faravelli, E. Ranzi, *Combust. Theor. Model.* 5 (2) (2001) 185–199.
- [45] A. Cuoci, A. Frassoldati, T. Faravelli, E. Ranzi, OpenSMOKE: Numerical modeling of reacting systems with detailed kinetic mechanisms, in: XXXIV Meeting of the Italian Section of the Combustion Institute, Rome, Italy, 2011.
- [46] G. Buzzi-Ferraris, *Scientific C++: Building Numerical Libraries the Object-Oriented Way*, Addison-Wesley, 1993.
- [47] G. Buzzi-Ferraris, BzzMath 6.0 Numerical Libraries, 2010, <<http://homes.chem.polimi.it/gbuzzi/index.htm>>.
- [48] M.D. Smooke, H. Rabitz, Y. Reuven, F.L. Dryer, *Combust. Sci. Technol.* 59 (1983) 295–319.
- [49] A. Frassoldati, R. Grana, T. Faravelli, E. Ranzi, P. Oßwald, K. Kohse-Höinghaus, *Combust. Flame* 159 (7) (2012) 2295–2311.
- [50] D.L. Baulch, C.J. Cobos, R.A. Cox, C. Esser, P. Frank, T. Just, J.A. Kerr, M.J. Pilling, J. Troe, R.W. Walker, J. Warnatz, *J. Phys. Chem. Ref. Data* 21 (1992) 411–429.
- [51] E. Ranzi, M. Dente, T. Faravelli, G. Pennati, *Combust. Sci. Technol.* 95 (1–6) (1994) 1–50.
- [52] R.P. Lindstedt, G. Skevis, *Combust. Sci. Technol.* 125 (1997) 73–137.
- [53] M. Frenklach, H. Wang, Soot formation in combustion: mechanisms and models, in: H. Bockhorn (Ed.), *Springer Series in Chemical Physics*, vol. 59, Springer-Verlag, Berlin, 1994, pp. 442–468.
- [54] S. Granata, S. Mancarella, F. Migliorini, M. Derudi, T. Faravelli, E. Ranzi, R. Rota, Formation of soot precursors in the rich combustion of hydrocarbon fuels, in: 10th International Congress on Combustion By-Products and their Health Effects, Ischia, June 17–20, 2007.
- [55] P. Frank, J. Herzler, T. Just, C. Wahl, *Proc. Combust. Inst.* 25 (1994) 833–840.
- [56] A. Fahr, S.E. Stein, *Symp. Int. Combust. Proc.* 22 (1989) 1023–1029.
- [57] E. Heckmann, H. Hippel, J. Troe, *Symp. Int. Combust. Proc.* 26 (1996) 543–550.
- [58] H. Wang, A. Laskin, N.W. Moriarty, M. Frenklach, *Proc. Combust. Inst.* 28 (2) (2000) 1545–1555.
- [59] Z.F. Xu, M.C. Lin, *J. Phys. Chem. A* 110 (2006) 1672–1677.
- [60] H.H. Grotheer, R. Louw, *Proc. Combust. Inst.* 26 (1996) 2405–2411.
- [61] R.D. Kern, K. Xie, *Prog. Energy Combust. Sci.* 17 (1991) 191–210.
- [62] S.H. Bauer, C.F. Aten, *J. Chem. Phys.* 39 (1963) 1253–1260.
- [63] M.B. Colket III, *Proc. Combust. Inst.* 21 (1986) 851–864.
- [64] A. Comandini, T. Malewicki, K. Brezinsky, *J. Phys. Chem. A* 116 (2012) 2409–2434.
- [65] R.S. Tranter, S.J. Klippenstein, L.B. Harding, B.R. Giri, X. Yang, J.H. Kiefer, *J. Phys. Chem. A* 114 (2010) 8240–8261.
- [66] S.H. Durrstein, M. Olzmann, J. Aguilera-Iparraguirre, R. Barthel, W. Klopper, *Chem. Phys. Lett.* 513 (2010) 20–26.
- [67] M.B. Colket, D.J. Seery, *Symp. (Int.) Combust.* 25(1) (1994) 883–891.
- [68] A. Comandini, K. Brezinsky, *J. Phys. Chem. A* 115 (2011) 5547–5559.
- [69] A.B. Lovell, K. Brezinsky, I. Glassman, *Int. J. Chem. Kinet.* 21 (21) (1989) 547.
- [70] M.C. Lin, A.M. Mebel, *J. Phys. Org. Chem.* 8 (1995) 407–420.
- [71] R. Butth, K. Hoyermann, J. Seeba, *Proc. Combust. Inst.* 25 (1994) 841–849.
- [72] Z. Zhao, M. Chaos, A. Kazakov, F.L. Dryer, *Int. J. Chem. Kinet.* 10 (2008) 1–18.
- [73] O. Herbinet, B. Husson, M. Ferrari, P.A. Glaude, F. Battin-Leclerc, *Proc. Combust. Inst.* 34 (1) (2013) 297–305.
- [74] J.T. Farrell, R.J. Johnston, I.P. Androulakis, Molecular Structure Effects on Laminar Burning Velocities at Elevated Temperature and Pressure, SAE Paper 2004-01-2936, 2004.
- [75] H. Bohm, D. Hesse, H. Jander, B. Luers, J. Pietscher, H.G. Wagner, M. Weiss, *Proc. Combust. Inst.* 22 (1988) 403–411.
- [76] M. Frenklach, *Phys. Chem. Chem. Phys.* 4 (2002) 2028–2037.
- [77] H. Richter, J.B. Howard, *Prog. Energy Combust. Sci.* 26 (4–6) (2000) 565–608.
- [78] M. Sirignano, A. D'Anna, *Proc. Combust. Inst.* 34 (1) (2013) 1877–1884.